Bioactive Materials 41 (2024) 158–173

Contents lists available at ScienceDirect

Bioactive Materials

journal homepage: www.keaipublishing.com/en/journals/bioactive-materials

Intrinsically bioactive multifunctional Poly(citrate-curcumin) for rapid lung injury and MRSA infection therapy

Tongtong Leng [a], Long Zhang [b,**], Junping Ma [a], Xiaoyan Qu [a,***], Bo Lei [a,b,*]

[a] Key Laboratory of Shaanxi Province for Craniofacial Precision Medicine Research, College of Stomatology, Frontier Institute of Science and Technology, Xi'an Jiaotong University, Xi'an, 710054, China
[b] Department of Respiratory and Critical Care Medicine, The Second Affiliated Hospital of Xi'an Jiaotong University, Xi'an, 710004, China

ARTICLE INFO

Keywords:
Bioactive materials
Bioactive polymers
Citrate polymer
Anti-inflammatory
Inflammatory diseases

ABSTRACT

Dysregulated inflammation after trauma or infection could result in the further disease and delayed tissue reconstruction. The conventional anti-inflammatory drug treatment suffers to the poor bioavailability and side effects. Herein, we developed an amphiphilic multifunctional poly (citrate-polyglycol-curcumin) (PCGC) nano oligomer with the robust anti-inflammatory activity for treating acute lung injury (ALI) and *Methicillin-resistant staphylococcus aureus* (MRSA) infected wound. PCGC demonstrated the sustained curcumin release, inherent photoluminescence, good cellular compatibility, hemocompatibility, robust antioxidant activity and enhanced cellular uptake. PCGC could efficiently scavenge nitrogen-based free radicals, oxygen-based free radicals, and intracellular oxygen species, enhance the endothelial cell migration and reduce the expression of pro-inflammatory factors through the *NF-κB* signal pathway. Combined the anti-inflammation and antioxidant properties, PCGC can shortened the inflammatory process. In animal model of ALI, PCGC was able to reduce the pulmonary edema, bronchial cell infiltration, and lung inflammation, while exhibiting rapid metabolic behavior *in vivo*. The MRSA-infection wound model showed that PCGC significantly reduced the expression of pro-inflammatory factors, promoted the angiogenesis and accelerated the wound healing. The transcriptome sequencing and molecular mechanism studies further demonstrated that PCGC could inhibit multiple inflammatory related pathways including *TNFAIP3*, *IL*-15RA, *NF-κB*. This work demonstrates that PCGC is efficient in resolving inflammation and promotes the prospect of application in inflammatory diseases as the drug-loaded therapeutic system.

1. Introduction

Many diseases such as rheumatoid arthritis, liver and lung injury are associated with the inflammation [1]. Inflammation is a defense reaction against injury and harmful stimuli, however, the excessive inflammation can cause the secondary tissue damage and dysfunction [2–6]. The process of inflammation is usually associated with the over-expression of pro-inflammatory factors and oxidative stress, which further aggravate the inflammatory response [6,7]. Anti-inflammatory therapy is generally considered to be an effective treatment for inflammatory diseases. The clinical treatment methods including antibiotics and systemic steroidal therapy, which aim to prevent the bacterial infection but not fix the disease [8–13]. Additionally, most of these drugs may have concerns on the side effects, including cardiovascular disease and liver and kidney toxicity [14–16]. It is crucial to develop innovative and effective strategy for regulating the inflammation and treating the related diseases.

Compared to the conventional treatment protocols, the bioactive polymers-based nano system possesses the special advantages including the large-scale fabrication and tailored structure-functions, which has become the promising strategy in regulating the inflammation environment [17–20]. Up to now, various polymers-based nanoparticles and

Peer review under responsibility of KeAi Communications Co., Ltd.
* Corresponding author. Frontier Institute of Science and Technology, Key Laboratory of Shaanxi Province for Craniofacial Precision Medicine Research, College of Stomatology, Xi'an Jiaotong University, Xi'an, 710054, China.
** Corresponding author.
*** Corresponding author.
E-mail addresses: longzhang@xjtu.edu.cn (L. Zhang), quxiaoyan@xjtu.edu.cn (X. Qu), rayboo@xjtu.edu.cn (B. Lei).

https://doi.org/10.1016/j.bioactmat.2024.07.002
Received 18 February 2024; Received in revised form 1 July 2024; Accepted 2 July 2024

nanovesicles have been developed and played a positive effect in anti-inflammatory treatment [21–23]. However, most of reported polymers-based nano systems showed the non-biodegradation or poor bioactivity or complicated synthesis, it is still necessary to develop the novel bioactive polymers nanosystem with the facile synthesis, controlled biodegradation, robust anti-inflammation and antioxidant activity, high biocompatibility, to treat the inflammatory diseases.

In recent years, as a typical bioactive synthetic polymer, polycitrate (PC) has attracted the much attention in regenerative medicine, due to their low cost, biocompatibility, and controlled biodegradability. PC-based polymers have been used in promoting retina/bone/muscle/skin tissue regeneration [24–28]. However, PC also possesses disadvantages

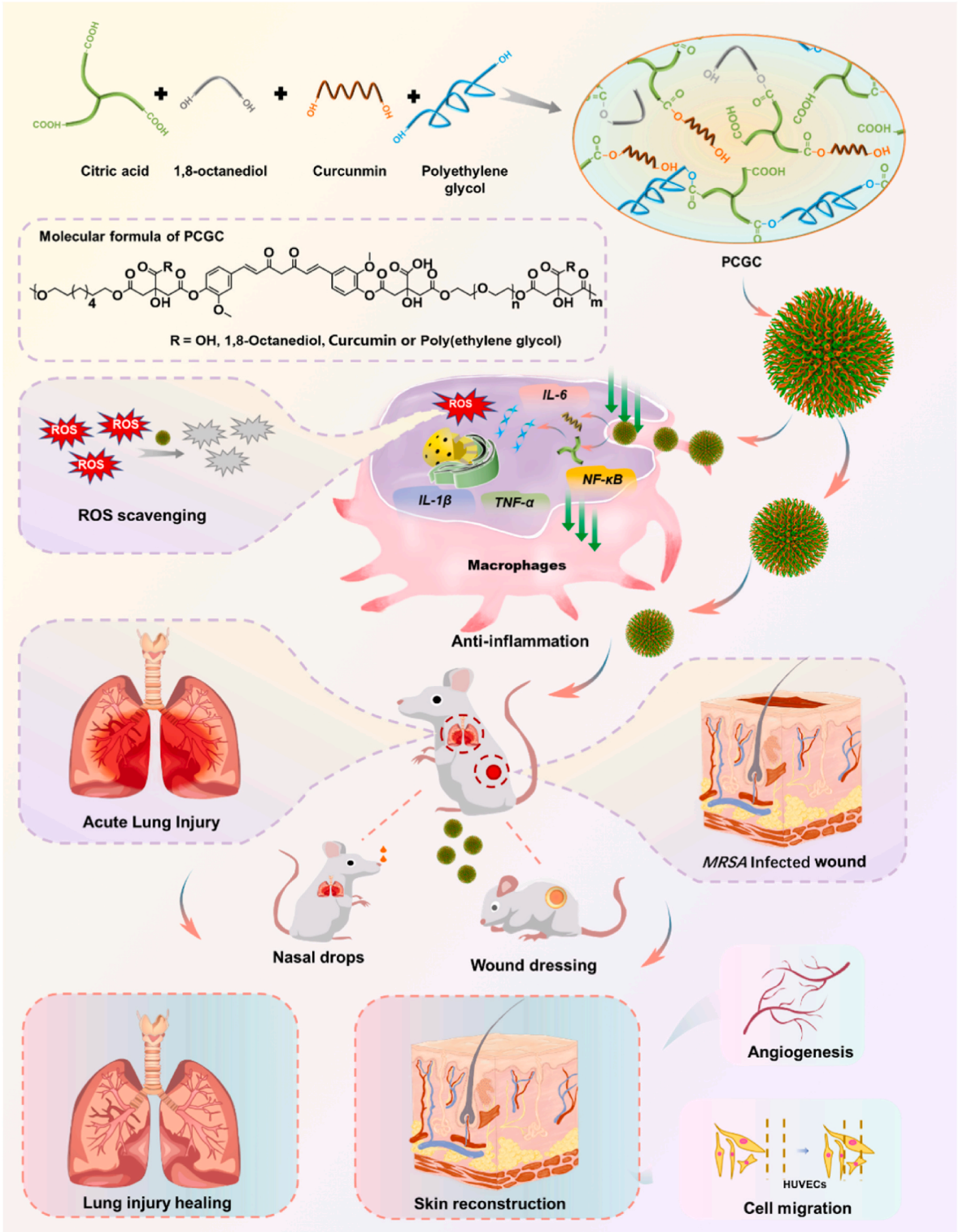

Scheme 1. Synthesis scheme of water-soluble polymeric nano oligomers of poly (citrate-polyglycol-curcumin) (PCGC). PCGC reduces the expression of pro-inflammatory factors *TNF-α*, *IL-6*, *NF-κB* and *IL-1β*. PCGC is effective scavenge ROS inside and reduce ROS-induced tissue damage. PCGC has shown good efficacy in animal models of acute lung injury (ALI) and *Methicillin-resistant staphylococcus aureus* (MRSA)-infected inflammatory wound.

such as low molecular weight, acidic degradation products and insufficient bioactivity [29–32]. To overcome the limitations of PC in regenerative medicine, our group reported a serious of strategies to develop the multifunctional PC-based polymers for extending their structure-functions and applications, including poly(citrate-silicon), poly(citrate-polyglycol), polycitrate-polyethylenimine and PC-based nanocomposites in bone, muscle and wound tissue regeneration [28,33,34]. The previous works also showed that functionalized PC could efficiently stimulate cell proliferation by activating mitochondria and regulate the inflammation through their antioxidant ability. In order to better expand the application of functionalized PC, the natural bioactive molecule could be as the monomer to synthesize activity-controlled polymers. There are many natural bioactive small molecules, such as polyphenols, flavonoids compounds, paclitaxel, camptothecin, etc. [35–38], and curcumin has always been well known for its excellent anti-inflammatory effect [39]. Curcumin is a natural phenolic substance with hypolipidemic, anti-tumor, anti-inflammatory, and antioxidant properties [40,41] In particular, previous studies have shown that curcumin has the same anti-inflammatory activity as some anti-inflammatory drugs, suggesting that curcumin has a good prospect in the field of inflammation treatment [42–44]. However, curcumin still has the limitations on low solubility, poor stability, low absorption rate and bioavailability [45–47]. The development of curcumin-based polymer can not only overcome the limitation but also improve the anti-inflammatory bioactivity of curcumin [48].

Herein, we report the amphiphilic multifunctional poly(citrate-polyglycol-curcumin) (PCGC) nanooligomers with the robust anti-inflammatory activity for treating acute lung injury (ALI) and *Methicillin-resistant staphylococcus aureus* (MRSA) infected wound. In this work, the PCGC was synthesized through a facile one-pot thermal polymerization route using citric acid, curcumin and polyglycol as the monomers (Scheme 1). In PCGC polymer, curcumin provides anti-inflammatory and antioxidant activity, citric acid can enhance the cell proliferation and PEG offers the amphiphilic property. The synthesis, structure, physicochemical properties, antiinflammation activity and potential mechanism, as well as the performance of ALI and MRSA-induced inflammatory wounds therapy, were investigated in detail.

2. Materials and methods

2.1. Synthesis and characterizations of PCGC

Poly(citrate-polyglycol-curcumin) (PCGC) was synthesized by the thermal polymerization in different molar ratios of citrate acid (CA) (Sigma), 1,8-octanediol (OD) (Aladdin), curcumin (Sigma) and polyethylene glycol (PEG) (Aladdin). PCGC with different feeding ratios was named as PCGC1% (CA:OD:curcunmin is PEG:1:0.693:0.007:0.3), PCGC2% (CA:OD:curcumin:PEG is 1:0.686:0.014:0.3), and PCGC5% (CA:OD:curcumin:PEG is 1:0.665:0.035:0.3), which were shown in the supporting information (Table S1). In addition, PCG (CA:OD:curcunmin: PEG = 1:0.7:0.3) without curcumin was synthesized as a control. The chemical structure of PCGC was characterized by ^{1}H nuclear magnetic resonance (^{1}H NMR) (Ascend 400 MHZ, Bruker) and Fourier transform infrared spectrum (FT-IR) (NICOLET 6700, Thermo). The morphological characteristics of PCGC were observed by transmission electron microscopy (TEM, JEM-2100Plus, JEOL) with 100 kV acceleration voltage. The particle size of PCGC was counted using Nano Measure software. The molecular weight of the PCGC polymer was measured by gel permeation chromatography (J2 GPC, PLTK) in the tetrahydrofuran phase. The zeta potential and polymer dispersity index (PDI) were test by Zeta sizer. The detailed synthesis procedure was shown in supporting information.

2.2. In vitro curcumin release and antioxidant evaluation

Specifically, 1 mL of PCGC aqueous solution (5 mg/mL) was loaded in a dialysis bag (MWCO 1000) and immersed in phosphate-buffered saline (PBS) pH 5.5 and 7.4 (9 mL). After different incubation times (4–72 h), the UV absorption value of the liquid outside dialysis bag was detected at 436 nm with ultraviolet–visible spectroscopy (*UV–VIS*) spectrometer (Lambda 35, PerkinElmer). In addition, the hydrolysates at 24 h, 48 h, and 72 h were analyzed by ultra performance liquid chromatography-quadrupole-time of flight-mass (UPLC-Q-TOF MS) spectrometry (WATERS I-Class VION IMS). Based on the absorbance standard curve, the release rate was calculated. The *in vitro* antioxidant properties of PCGC were tested by the 1,1-diphenyl-2-picrohydrazine (DPPH·) method according to the procedure in supporting information. The ability of PCGC to scavenge superoxide anion ($O_2^{\bullet-}$) free radicals was measured by the superoxide dismutase (SOD) kit.

2.3. Fluorescence property detection

The photoluminescent properties including excitation and emission spectra were carried out by a steady state and transient fluorescence spectrometer (FLS9, Edinburgh) at room temperature. The emission spectra of PCG and PCGC were tested by dissolving them in H_2O (30 mg/mL). The fluorescence characteristics of PCGC were evaluated by measuring emission spectra at different excitation wavelengths.

2.4. Hemocompatibility and cytotoxicity analysis

The hemocompatibility of samples was determined through testing the absorbance of the supernatant of the erythrocytes solution at 540 nm after incubation with PCGC. The 0.1 % Triton X-100 and PBS as negative and positive control. The Alamar Blue kit (Invitrogen) was selected to investigate the effect of PCGC on the activity of mouse fibroblasts (L929), mouse leukemia cells of monocyte macrophage (RAW 264.7) and human umbilical vein endothelial cells (HUVECs). The proportion of viable cells was detected by a microplate reader (530 nm/600 nm, SpectraMax Paragigm, Molecular Equipment). The methods of hemocompatibility and cytotoxicity analysis of PCGC were shown in supporting information.

2.5. Cellular uptake capacity of PCGC in macrophages

A total of 1×10^4 RAW 264.7 cells were seeded on 24-well cell slides, curcumin (3 μg/mL) and PCGC (100 μg/mL) were co-cultured with RAW 264.7 cells for 24 h. Then, the cells were washed 3 times with PBS. The cell nuclei were stained with DAPI, and the fluorescence of DAPI was excited at 405 nm to mark the position of the nucleus (blue) and the fluorescence of PCGC (red) was excited at 488 nm. The fluorescent images were taken by confocal laser scanning microscopy (FV 1200, Olympus) and photographed. In addition, the cellular uptake capacity of PCGC in macrophages was detected by a flow cytometry. The specific experimental method was shown in supporting information.

2.6. Endothelial cell migration analysis

HUVECs were seeded in 24-well plates at a density of 1×10^4 cells/well. A slit approximately 1.5 mm wide was drawn in the middle of each well and washed with PBS three times so that there were no cells in the slit. The cells were cultured using medium (DMEM with 2 % fetal bovine serum, GIBCO) under standard conditions (humid environment, 5 % CO_2, 37 °C). In a low serum environment, the proliferation of cells is inhibited, and more cells perform migration behavior, which can reduce the error of migration experiments caused by cell proliferation. The cells were co-cultured with the materials, and the migration of cells to the gap was observed and recorded at 24 h, 48 h and 72 h. The gap width was measured using a Nano Measurer software, and the mobility was calculated.

2.7. Anti-inflammatory activity and intracellular antioxidant evaluation

Real-time quantitative polymerase chain reaction (RT−PCR) was used to study the expression of interleukin-1β (*IL-1β*), interleukin-6 (*IL-6*), nuclear factor kappa-B (*NF-κB*) and tumor necrosis factor (*TNF-α*) in lipopolysaccharide (LPS)-treated RAW 264.7 cells after incubation with different materials. Immunofluorescence staining was used to study the protein expression of TNF-α in RAW 264.7 cells after treatment with different materials. The fluorescence of proteins was then observed by the confocal laser scanning microscopy, the fluorescence intensity was counted using Image J software. 2,7-Dichlorodihydrofluorescein diacetate (DCFH-DA) (Sigma) was used to detect the content of reactive oxygen species (ROS) in RAW 264.7 cells. The detailed experiment process was shown in the supporting information. The expression of NF-κB protein was analyzed by the western-blot, which was commissioned to Shaanxi Yike Biotechnology Service Co., Ltd.

2.8. In vivo acute lung injury model and toxicity evaluation

Bal b/c mice (male, 17 g–21 g) were selected for acute lung injury (ALI) modeling. Mice were randomly divided into the following 5 groups (n = 4): normal control group (NC), LPS + PBS group, LPS + PCG group, LPS + curcumin group and LPS + PCGC group. Mice were gas anesthetized with isoflurane, and LPS was added dropwise at a rate of 6 mg/kg through nasal drops. After 2 h, the mice were anesthetized with isoflurane again, the material was dripped at a ratio of 5 mg/kg by nasal drip for treatment, and PBS was dripped as a negative control. After 18 h of treatment, the mice were decapitated and killed by de-neck, the bronchoalveolar lavage fluid was collected with PBS, and the number of cells in the bronchoalveolar lavage fluid was counted using a hemocytometer. Then, the lungs were dissected and collected for H&E staining. In immunohistochemical staining, NF-κB antibody was used as a marker of inflammation. In addition, the lung tissues of ALI mice treated with different materials were frozen in liquid nitrogen and then the sections were subjected to ROS immunofluorescence staining to verify the ROS scavenging effects of different materials *in vivo*. The ear thermometer was used to measure deep abdominal temperature in mice before and 2, 15, 18, and 20 h after modeling. All animal experimental procedures were performed in accordance with the procedures approved by the Animal Care Committee of Xi'an Jiaotong University (2019-1167). After treatment of the ALI model, the liver and kidney tissue of the mice were collected, and the morphology of the liver and kidney tissue was observed by H&E staining.

2.9. In vivo metabolism evaluation

The fluorescent dye Cy7 was linked to PCGC by amidation reaction, and then PCGC was dripped into ALI mice by nasal drops, with the same dose as in ALI animal experiments. After the mice were killed by de-neck, the heart, liver, spleen, lung, and kidney were obtained, and the fluorescence intensity of each organ at 748 nm was observed using a small animal fluorescence imaging system.

2.10. MRSA infected wound model

Kunming mice (female, 30–35 g) were selected for the *in vivo Methicillin-resistant staphylococcus aureus* (MRSA)-infected inflammatory wound healing model. Mice were randomly divided into the following 4 groups (n = 4): control group (blank), PCG group, curcumin group and PCGC group. The detailed process was according to the previous reports [38]. On day 3, 7, and 12, according to the manufacturer's protocol, all samples were collected and stained with H&E. In immunohistochemical staining, vascular endothelial growth factor (VEGF) antibody was used as a marker of wound angiogenesis, and TNF-α antibody was used as a marker of inflammatory factors. Then, the sections were observed by an optical microscope (BX53, Olympus, Japan). The detailed experiment process was shown in the supporting information.

2.11. RNA-sequencing analysis

The potential molecular mechanism of PCGC regulating phenotypic changes of macrophages during inflammation was detected by the transcriptome sequencing. Specially, LPS-treated RAW 264.7 cells were incubated with PCGC for 48 h, and LPS group was used as negative control. RNA was extracted using the Trizol method (Invitrogen, CA, USA). Sequencing was performed on Illumina Novaseq 6000 completed by Beijing Allwegene Tech. (project number: AWGT22112102).

2.12. Statistical analysis

All experiments were independently repeated at least three times. The data are expressed as the mean ± standard deviation (SD). The statistical significance of the difference between groups was assessed by the student's *t*-test. $^{*}p < 0.05$, $^{**}p < 0.01$ were considered to be statistically significant.

3. Results and discussion

3.1. Synthesis and characterizations of PCGC

Poly (citrate-polyglycol-curcumin) (PCGC) was synthesized by a facile one-pot thermal polymerization process (Scheme 1, Fig. S1). To show the effect of curcumin on the structure and properties, PCGC with different content of curcumin was synthesized, named as PCGC1%, PCGC2%, and PCGC5% respectively. And PCG (without curcumin) was synthesized as a control. After testing, it was found that the curcumin addition amount in PCGC5% is the maximum value. If too much curcumin is added during the reaction, it will precipitate. Fig. 1A and B shows the chemical structure characterization of PCGC. According to the ^{1}H NMR results (Fig. 1A), CA has several characteristic peaks (–CH_2–) between 2.6 and 3.0 ppm, 1.2, 1.5, 3.9 and 4.1 ppm is OD's representative methylene (–CH_2–) absorption peak, the peaks at 7–8 ppm are the hydrogens on the phenyl ring of curcumin and the representative methylene group (–CH_2–), and the methylene (–CH_2-) characteristic peaks of PEG appear at 3.5, 4.2, and 4.3 ppm. Different peak areas were integrated, and the grafting rate of curcumin were calculated (Tables S1 and 2). After calculation, it was found that 1 mol of PCGC1%, PCGC2%, and PCGC5% contained 0.006, 0.011, and 0.033 mol of curcumin respectively. The actual curcumin graft ratio was slightly lower than the theoretical molar ratio, indicating that the speculative OD and curcumin may not be fully reacted.

The chemical structure of PCGC was further confirmed by Fourier transform infrared (FT-IR) spectroscopy (Fig. 1B). A doublet of the methylene group (–CH_2–) of OD appears at 2800-3000 cm^{-1}, pure curcumin has a phenolic hydroxyl peak at 3503 cm^{-1}, which disappeared in PCGC, indicating that the phenolic hydroxyl group was reacted, further indicating that curcumin was successfully connected to the main chain. Moreover, the molecular weight of PCGC5% was 1554 g/mol (Mn) and 2400 g/mol (Mw) with a polydispersity of 1.5444, and the Mn and Mw of PCG, PCGC1%, and PCGC2% are shown in the supplemental information (Table S3). Curcumin has the poor water solubility, low bioavailability and slight cytotoxicity, which greatly limited its application [46]. In this study, the curcumin could be released slowly from PCGC as their degradation, which could improve its utilization and its biological safety. Fig. 1C shows the *in vitro* curcumin release at pH 7.4 environment. Curcumin was slowly released from the PCGC polymer within 70 h. In addition, the hydrolyzate of PCGC was analyzed and the release of curcumin could be seen at 24 h, 48 h and 72 h (Fig. S2). When used to treat inflammation, the PCGC is expected to continuously release curcumin *in vivo,* to achieve long-term anti-inflammatory treatment.

In the TEM image, it's possible to observe that PCGC nanooligomers possesses circular shape with a size of approximately 42 nm (Fig. 1D and

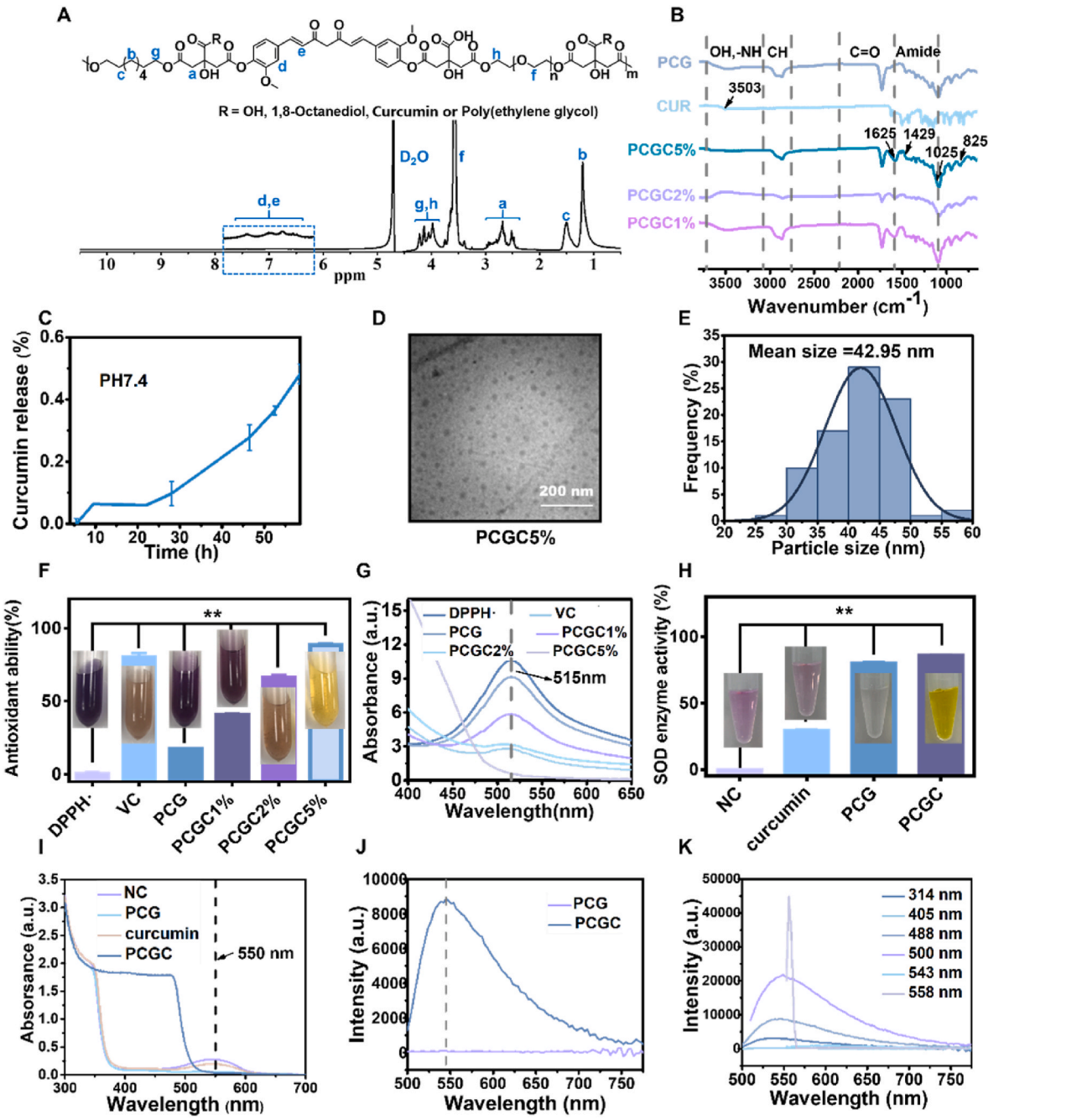

Fig. 1. Chemical structure, *in vitro* release, antioxidant properties and fluorescence properties of PCGC. (A) Chemical structural formula and ^{1}H NMR spectrum of PCGC. (B) FTIR spectra indicating the formation of PCGC structures. (C) Curcumin release rates from PCGC in pH 7.4 environments. (D) TEM images of PCGC5%. (E) Particle size statistics of PCGC nano oligomers. (F) Optical photos and statistical data of antioxidant capacity *in vitro*. $^{*}p < 0.05$ and $^{**}p < 0.01$, n = 4. (G) UV absorption spectra of DPPH· treated with different materials. (H) Optical photos and statistical data of SOD enzyme activity *in vitro*. $^{*}p < 0.05$ and $^{**}p < 0.01$, n = 4. (I) UV absorption spectra of superoxide anion ($O_2^{\bullet-}$) treated with different materials. (J) Fluorescence emission spectra of PCGC and PCG excited at 488 nm. PCGC showed significantly enhanced photoluminescent ability as compared with PCG. (K) Fluorescence emission spectra of PCGC at different excitation wavelengths.

E). In addition, Zeta sizer was used to measure the zeta potential and polymer dispersity index (PDI) of PCGC in DI water, phosphate-buffered saline (PBS), DMEM, and DMEM+10 % Fetal Bovine Serum (FBS) (Figs. S3A and B). PCGC showed similar zeta potential and PDI in various solutions. In general, the zeta potential values of PCGC in different solutions were about −2 to −5 mv (Fig. S3A), and the PDI was about 0.35–0.65 (Fig. S3B). PCGC showed good stability in different solutions.

3.2. *In vitro* antioxidant and fluorescent properties of PCGC

When the inflammation occurs, there an imbalance in the regulation of oxidation and antioxidant activity in cells, resulting in the production of a large number of free radicals under physical and chemical effects [49–51]. Free radicals can aggravate inflammation, promoting the production of more free radicals, becoming a vicious cycle that prolongs the course of inflammation [52]. Since both curcumin and PC have antioxidant properties, which can scavenge free radicals and reduce oxidative damage, so the PCGC *in vitro* antioxidant capacity was studied.

The scavenging activity of PCGC on nitrogen radicals was investigated by testing the scavenging efficiency of 1,1-diphenyl-2-picrylhydrazine (DPPH·) (Fig. 1F and G). The optical photos showed, compared with the DPPH· group, that the color of the PCGC group was significantly lighter, suggesting the clearance of DPPH·. The clearance rates of PCGC1%, PCGC2% and PCGC5% were 40.6 ± 0.9 %, 65.9 ± 2.3 % and 88.5 ± 1.3 %, respectively, which were significantly higher than those of the Vitamin C (VC) group and PCG group (Fig. 1F).This result indicates that the addition of curcumin further enhances the scavenging ability of PCGC for nitrogen radicals. It can also be seen in the UV spectrum that the characteristic absorption peak of DPPH· at 515 nm in PCGC group was significantly lower than that of DPPH· group (Fig. 1G). Further analysis to determine the scavenging ability of PCGC to other types of free radicals, the superoxide dismutase (SOD)-like enzyme activity of PCGC was performed, and the results showed that PCGC has excellent SOD-like enzyme activity. From Fig. 1H, it can be seen that the PCG and PCGC groups have obvious scavenging effects on superoxide anion ($O_2^{\bullet-}$), which is reflected in the obvious lighter purple color of the solutions in these group. After measuring its SOD enzyme activity, it was found that PCGC has the strongest SOD enzyme activity, which is significantly higher than the other three groups. It can also be found the absorption peak of superoxide anion ($O_2^{\bullet-}$) of PCGC group at 550 nm disappeared (Fig. 1I), showing excellent free radicals scavenging and antioxidant capabilities, indicating the good antioxidant capacity of PCGC and the potential application against oxidation stress in cells.

Previous studies have shown that curcumin has fluorescence emission properties in multiple bands, which could be used to observing the cellular uptake of PCGC. Therefore, the fluorescence properties of PCGC *in vitro* were studied (Fig. 1J and K). Without adding any fluorescent dyes or quantum dots, PCGC still showed the significant photoluminescence. Under 488 nm excitation, compared with PCG, the fluorescence emission of PCGC was significantly increased (Fig. 1J). In addition, at different excitation wavelengths (314 nm, 405 nm, 500 nm, and 558 nm), the fluorescence emission peak position of PCGC shifted. (Fig. 1K). The fluorescence property of PCGC makes it possible to conduct real-time fluorescence imaging, locate and track the conversion

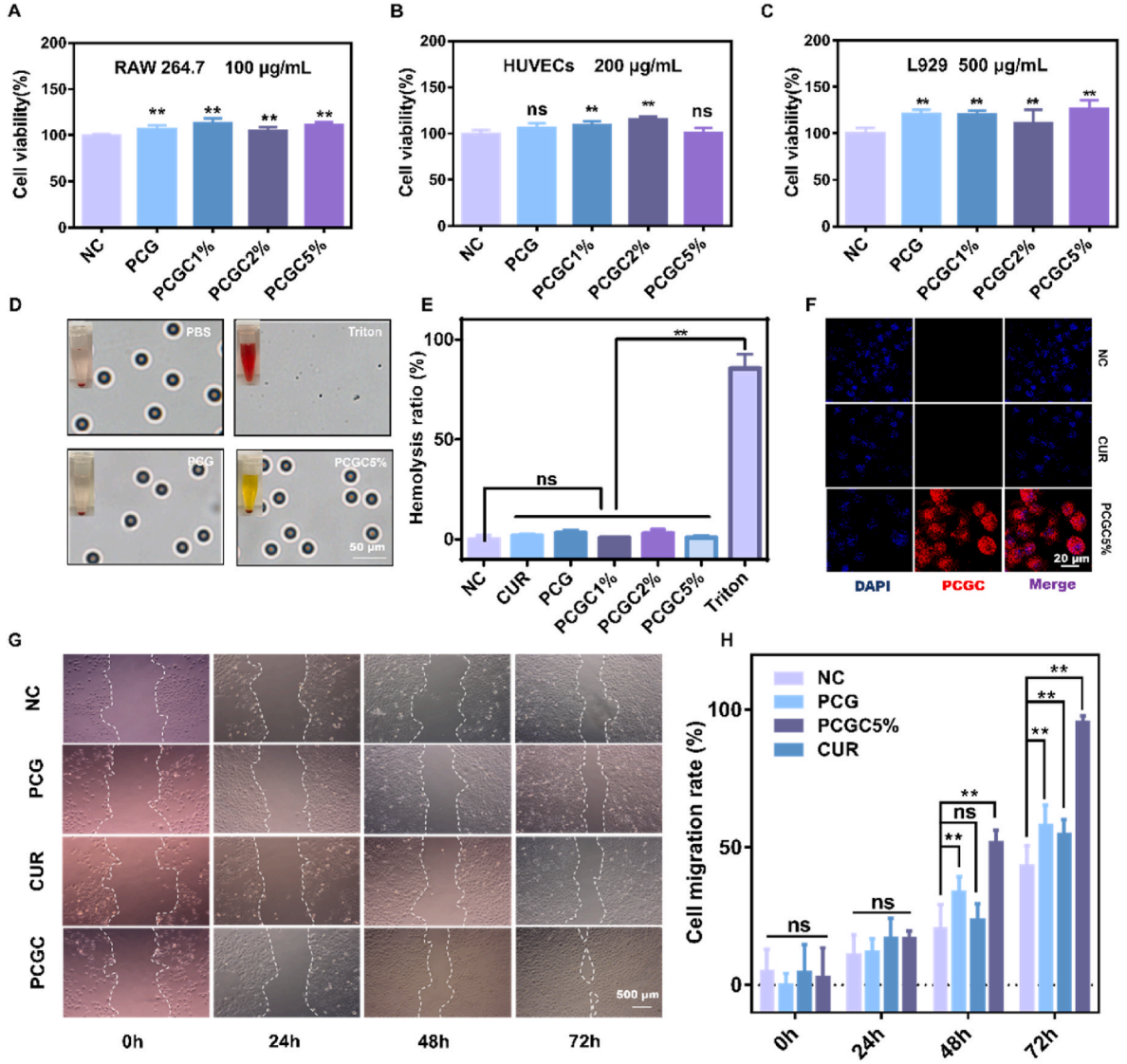

Fig. 2. Hemocompatibility, cytocompatibility evaluation, cell uptake capacity, and cell migration promoting properties of PCGC. (A–C) Statistics of cell viability of different cells treated with different materials for 24h. (A) RAW 264.7 cells. (B) HUVECs. (C) L929 cells. (D) Optical photographs of the hemocompatibility test of different materials and photographs of red blood cell morphology observed under a microscope during hemocompatibility testing. (E) Statistics of hemocompatibility of different materials. (F) Fluorescence photos of RAW 264.7 cells' uptake of different materials, red channels showing PCGC, and sections counterstained with DAPI (blue). (G) Optical photos of cell migration after HUVECs were treated with different materials for 24 h, 48 h and 72 h. (H) Statistics of the effect of different materials on the cell mobility of HUVECs. $^*p < 0.05$ and $^{**}p < 0.01$, n = 4.

process of biomaterials in inflammation treatment.

3.3. In vitro biocompatibility and cellular uptake capacity assessment

To determine the *in vitro* biosafety of PCGC, the cytotoxicity against mouse leukemia cells of monocyte macrophage (RAW 264.7), fibroblasts (L929), endothelial cells (HUVECs) and blood cells was investigated (Fig. 2A–E, Fig.S4). After co-culturing PCGC with these three kinds of cells for 24 h, the safe concentrations of PCGC in RAW 264.7, HUVECs and L929 cells were 100 μg/mL, 300 μg/mL and 500 μg/mL respectively (Fig. 2A–C).

Fig. 2D and E shows the results of hemocompatibility of PCGC. The Triton group as a negative control exhibited obvious hemolysis with the red supernatant. The PCGC group was the same as the PBS group, and the erythrocytes settled at the bottom of the centrifuge tube and the supernatant was clarified (Fig. 2D). Afterwards, the erythrocyte morphology was observed under the microscope and found that the erythrocytes in the PBS, PCGC and PCG groups had a complete shape and were healthy biconcave circles, while in the Triton group, due to the rupture of erythrocytes, only some cell debris could be seen under the microscope (Fig. 2D). Then the hemolysis rate was calculated (Fig. 2E). The hemolysis rates of the PCGC1%, PCGC2%, and PCGC5% groups were all lower than 5 %, indicating that PCGC has good hemocompatibility.

Previous studies have shown that curcumin generally played a role outside cells and cannot be taken up by cells, which makes them easier to remove, with a short circulation time in the body and a low utilization rate [53,54]. Probably PCGC polymers are more easily taken up by cells due to their nanoscale size and can enter cells to play a direct role, thereby prolonging the action time and improving utilization. The results show that RAW 264.7 cells can take up PCGC very well (Fig. 2F). Specially, the results showed that the red fluorescence emitted by PCGC in RAW 264.7 cells in the PCGC group coincided with the position of the nucleus stained with DAPI (blue), and the red fluorescence of PCGC was observed in all cells, proving that RAW 264.7 cells had good uptake of PCGC, while the curcumin group had no fluorescence emission at 488 nm, indicating that curcumin could not be taken up by RAW 264.7 cells, which was the same as our assumption. Moreover, the cellular uptake capacity of PCGC by RAW264.7 cells was tested by flow cytometry. The results showed that more cells in the PCGC group detected strong fluorescence signals at 488 nm (Fig. S5), which was consistent with the results shown in the fluorescence photo, proving that PCGC can be well cellular uptake by macrophages.

3.4. Cell migration effect of PCGC

In the later stages of wound healing, endothelial cell migration plays an important role in angiogenesis [55,56]. To explore whether PCGC has the properties of promoting endothelial cell migration, HUVECs was used to conduct scratch experiments. It was proven that PCGC promoted the endothelial cell migration (Fig. 2G and H). Specifically, after 24 h co-culturing, there was no significant difference in scratch width among the groups. After 48 h, the average cell migration rates of the NC (normal control), PCG, curcumin and PCGC groups were 20.5 %, 33.8 %, 23.7 % and 52 %, respectively. After 72 h, the average cell migration rates of the NC, PCG, curcumin and PCGC groups were 43.5 %, 58.1 %, 54.9 % and 95.6 %, respectively. This result indicated that PCGC could significantly enhance the HUVECs migration, suggesting their positive effect on the angiogenesis.

3.5. Intracellular antioxidant activity

In the process of inflammation, accompanied by an imbalance of oxidation and antioxidant activity, macrophages produce reactive oxygen species (ROS) during the inflammatory process to kill bacteria [57]. However, too much ROS can cause secondary damage to tissues, the scavenging the intracellular ROS could efficiently regulates the inflammation response. Here, the *in vitro* the ROS scavenging effect of PCGC in RAW 264.7 cells were evaluated. The results demonstrate that PCGC has an excellent intracellular ROS scavenging effect (Fig. 3A and B). Specifically, ROS production in RAW 264.7 cells increased after LPS treatment of 48 h, as shown as the green fluorescence (Fig. 3A). Compared with the LPS group, the ROS content of the LPS + PCG, LPS + curcumin, and LPS + PCGC groups was significantly decreased (Fig. 3B). In particular, ROS in the LPS + curcumin and LPS + PCGC groups was almost completely eliminated. The results of intracellular and *in vitro* antioxidant experiments suggested that PCGC has good antioxidant capacity and can have an excellent curative effect in the treatment of inflammation.

3.6. Anti-inflammatory activity

To investigate the therapeutic potential of PCGC for inflammatory diseases, the effect of PCGC on LPS treated RAW 264.7 cells was investigated (Fig. 3C–F). *TNF-α*, *IL-6*, *NF-κB* and *IL-1β* are several common pro-inflammatory factors that play an important role in the occurrence of inflammation [58]. The effect of PCGC on the expression of pro-inflammatory factors at the gene level was explored. The optimal anti-inflammatory concentration of PCGC was screened out through the preliminary experiments (100 μg/mL) (Fig. S6), and the anti-inflammatory activity of PCGC was studied based on this concentration. Compared with the NC group, the expression of *TNF-α*, *IL-6*, *NF-κB* and *IL-1β* in LPS group was increased after 24 h of LPS treatment (Fig. 3C–F). The expression of *TNF-α*, *IL-6*, *NF-κB* and *IL-1β* was significantly decreased in RAW 264.7 cells after incubation with PCGC for 48 h. Specifically, the expressions of *TNF-α*, *IL-6*, *NF-κB* and *IL-1β* in the LPS + PCGC group were significantly lower than those in the LPS group and the expressions of *IL-6*, *NF-κB* and *IL-1β* were significantly lower than those in the LPS + PCG group. In particular, the expression levels of *TNF-α* and *NF-κB* in LPS + PCGC group were significantly lower than those in the LPS + Dexamethasone (DEX) group (positive control) (Fig. 3C and E). These results show that PCGC can inhibit the expression of *TNF-α*, *IL-6*, *NF-κB* and *IL-1β*, and the addition of curcumin enables PCGC to better inhibit the expression of pro-inflammatory factors at the gene level.

To further verify the inhibitory effect of PCGC on inflammation, the immunofluorescence staining of TNF-α protein was performed (Fig. 3G and H). The results show that the fluorescence of TNF-α in NC, LPS + DEX, LPS + curcumin, and LPS + PCGC groups were weak, while the fluorescence of LPS group was strongest. After statistical analysis of fluorescence intensity, the results showed that compared with the NC group, the expression of TNF-α protein in LPS group was significantly increased after stimulation with LPS. After treatment with different materials, the TNF-α protein expression in the LPS + DEX group, LPS + PCGC, LPS + PCG and LPS + curcumin groups significantly decreased. Compared with the LPS group, the expression levels of TNF-α protein in LPS + DEX, LPS + PCG, LPS + curcumin and LPS + PCGC groups were 31.4 %, 45.4 %, 58.7 % and 17.3 %, respectively. The expression of TNF-α protein in the LPS + PCGC group was the lowest, even lower than that in the LPS + DEX group, which proved that PCGC could significantly inhibit the expression of TNF-α at the protein level. In addition, the expression level of NF-κB protein level was verified by Western blot (Fig. 3I). The results showed that the expression level of NF-κB in the PCGC group was consistent with that in NC group, indicating that PCGC reduced the expression level of NF-κB, showing the excellent anti-inflammatory effect.

During the development of inflammation, macrophages undergo two types of polarization, polarizing into two cell subtypes: M1 and M2. It is generally thought that M1 type cells play a pro-inflammatory role in the inflammatory process, so they are important in anti-inflammatory processes [59]. In the treatment of inflammation, it is generally hoped to inhibit the polarization of macrophages towards the M1 type. In order to

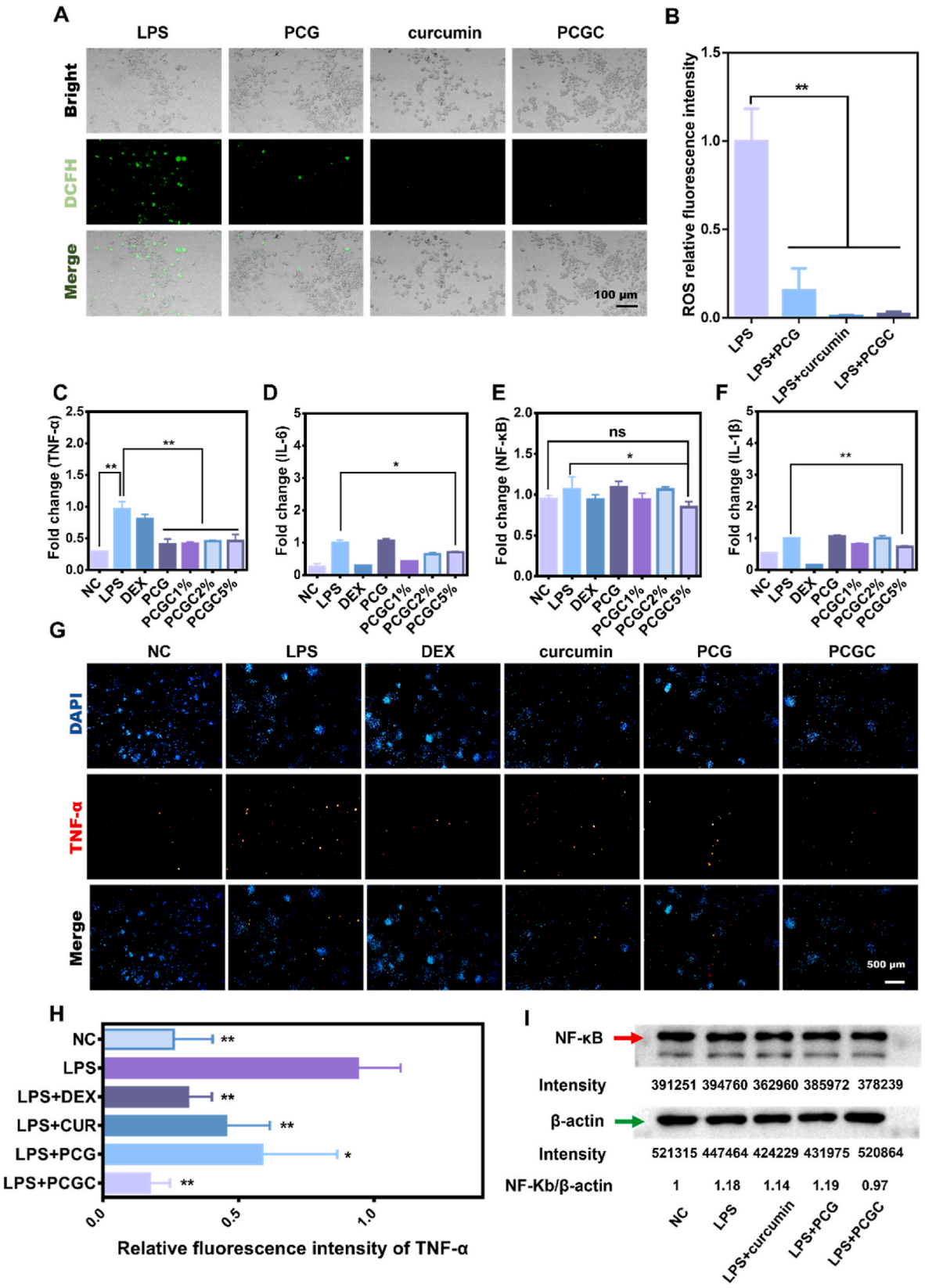

Fig. 3. Antioxidant and anti-inflammatory properties of PCGC. (A) Fluorescence photos after intracellular ROS staining with DCFH-DA, the green channel shows ROS. (B) Corresponding statistics of fluorescence intensity of ROS. (C–F) Statistics of the expression of *TNF-α, IL-6*, *NF-κB* and *IL-1β* detected by real-time PCR. (G) Immunofluorescence staining for intracellular TNF-α protein, the red channel shows TNF-α expression, while the section is counterstained with DAPI. (H) Corresponding statistics of fluorescence light intensity of TNF-α protein. $^{*}p < 0.05$ and $^{**}p < 0.01$, n = 4. (I) Western blot analysis of NF-κB protein expression in RAW 264.7 treated with different materials.

explore the impact of PCGC on macrophages (RAW 264.7), CD86 antibody was used to label M1 macrophages and then the proportion of M1 macrophages was detected by flow cytometry. The results shows that PCGC can inhibit polarization of macrophages toward the M1 pro-inflammatory type. Specifically, the proportion of M1 macrophages in RAW 264.7 without LPS-induced polarization (NC group) was 54.67 % (Fig. S7A). After LPS-induced polarization, the proportion of M1 macrophages in the LPS group reached 71.93 % (Fig. S7B). After treatment, the proportions of M1 macrophages in the LPS + CUR, LPS + PCG and LPS + PCGC groups were 69.87 %, 69.66 % and 65.27 % respectively (Figs. S7C–E). The proportion of M1 macrophages in the PCGC5% group was lower than that in the other groups, proving that PCGC can effectively inhibit M1 type polarization, thereby suppressing inflammation. In summary, PCGC can inhibit the expression of pro-inflammatory factors at the gene and protein levels, and inhibit polarization of macrophages toward the M1 pro-inflammatory type, thereby exerting an excellent anti-inflammatory effect and effectively inhibiting the inflammatory process.

3.7. Acute lung injury treatment

Acute lung injury (ALI) can result in respiratory failure among patients, and anti-inflammatory therapy is a viable treatment strategy for ALI [60,61]. The acute inflammation model of LPS-induced ALI was selected to investigate the anti-inflammatory effect of PCGC *in vivo* (Fig. 4A). Before the formal experiment, preliminary experiments were conducted to select the optimal therapeutic concentration of PCGC, and finally determined that the dose of 5 mg/kg can achieve the best therapeutic effect. The specific experimental results are shown in the supporting information (Fig. S8A). After 14 h of PCGC treatment, lung volume of mice in the LPS + PCGC group were smaller (Fig. 4B). Specifically, under acute inflammation, the permeability of the alveolar wall changes, and the infiltration of tissue fluid leads to acute edema in the lungs, which can be seen from the appearance of a significant increase in the volume of the lungs [62]. As shown in Fig. 4B, the lung volume of the NC group was smaller, and the lung volume of the LPS + PBS (negative control) was significantly increased. The lung volume of the LPS + PCGC group was significantly reduced. Then the lung size was statistically analyzed, and it was found that the lung size of the LPS + PCGC group was significantly smaller than that of the LPS group

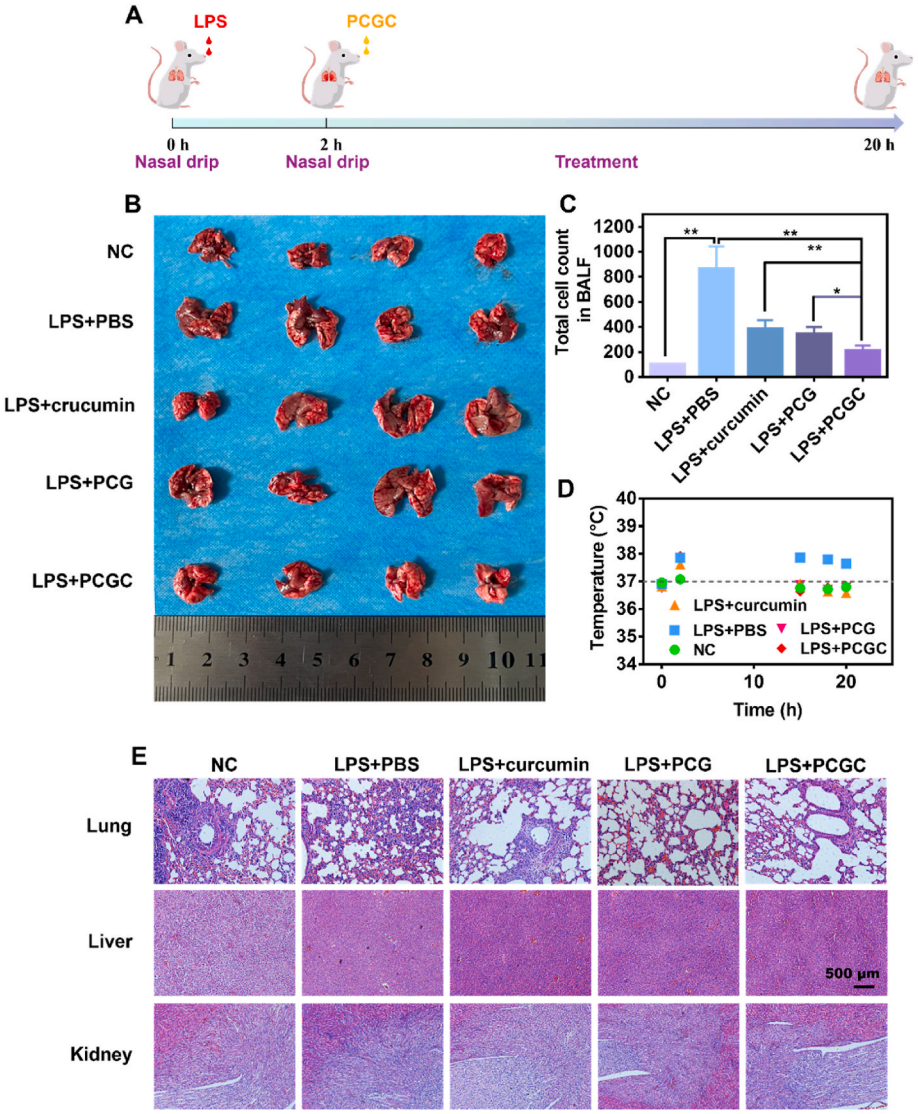

Fig. 4. Acute lung injury (ALI) model assessment. (A) Schematic diagram of mice ALI model. (B) Optical photos of lung volume of ALI model mice treated with different materials. (C) Total cells count in bronchoalveolar lavage fluid of ALI model mice. $^{*}p < 0.05$ and $^{**}p < 0.01$, n = 4. (D) Body temperature of ALI model mice within 20 h. (E) H&E staining of lung, liver and kidney tissues of ALI model mice.

(Fig. S8C), proving that pulmonary edema was significantly weakened. In addition, the changes in the permeability of the alveolar wall caused by acute inflammation can cause inflammatory cells to infiltrate the alveolar bronchi [63]. Bronchoalveolar lavage was performed and total cells in the bronchoalveolar lavage fluid were counted. The results showed that the total number of cells in the LPS + PBS group was much higher than that in the NC group, showing strong cell infiltration. The total cell numbers in the LPS + curcumin, LPS + PCG and LPS + PCGC groups all decreased significantly, and the LPS + PCGC group had the lowest total cell number compared with the other treatment groups, proving that PCGC had the best effect in reducing cell infiltration (Fig. 4C). Correspondingly, the body temperature of mice increased during acute inflammation. After modeling, the body temperature of mice in all groups except for the NC group showed an increase, while that of mice in the LPS + PBS group remained at approximately 38 °C. After treatment, the body temperature of mice in the LPS + curcumin, LPS + PCG, and LPS + PCGC groups was basically the same as that in the NC group (Fig. 4D).

Moreover, the lung status of mice was observed through H&E-stained sections of the lungs. The results showed that dense inflammatory cell infiltration and thickening of alveolar walls appeared around the airways of mice in the LPS + PBS group. After PCGC treatment, the infiltration of inflammatory cells was also reduced, the alveolar walls became thinner, and inflammation was significantly reduced (Fig. 4E). At the same time, to verify the safety of PCGC in the treatment of ALI, the liver and kidney of mice administered PCGC by nasal drop were took and performed H&E staining, which showed no discernible microstructural disruption or inflammatory cell infiltration following PCGC treatment. Although comprehensive studies are required to fully demonstrate its *in vivo* safety, intranasal PCGC at this therapeutic dose did not cause liver and kidney damage (Fig. 4E).

As mentioned in previous studies. PCGC can effectively scavenge ROS *in vitro* and in cells. The scavenging effect of PCGC on ROS *in vivo* was verified. The results showed that PCGC can effectively scavenge ROS *in vivo* and achieve a super strong antioxidant effect (Fig. 5A). Specifically, it can be observed that in the immunofluorescence staining results of ROS (red channel) in the lung sections of mice in the non-modeled group (NC group), no obvious red fluorescence can be seen, while in ALI mice modeled by LPS, obvious red fluorescence can be observed around the lung airways, showing more ROS aggregation. After treatment, the red fluorescence in the PCG and curcumin groups weakened, especially the PCGC group had the lowest ROS fluorescence intensity, almost equivalent to the NC group, showing the best ROS scavenging effect, which is consistent with previous *in vitro* research results, proving that PCGC has excellent antioxidant capacity.

To determine the therapeutic effect of PCGC on ALI, immunofluorescence staining on the NF-κB protein in the lungs of mice were performed to observe the inflammatory state of the lungs. The results showed that after PCGC treatment, the expression of NF-κB protein in the lungs of mice was significantly reduced (Fig. 5B). Specifically, it can be seen that the green fluorescence of NF-κB in the lungs of the unmodeled NC group mice was less, while the cells around the airways

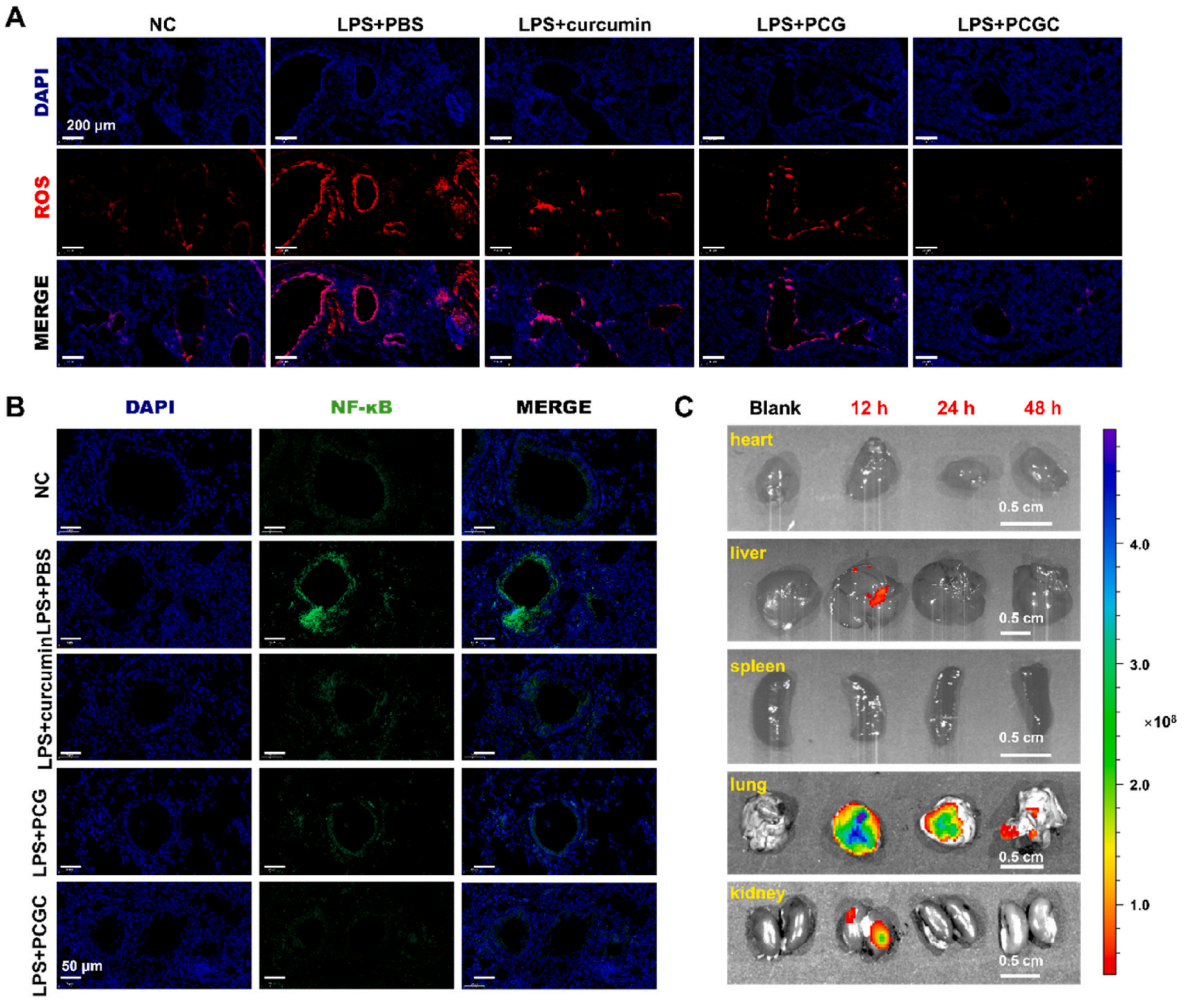

Fig. 5. Acute lung injury (ALI) evaluation. (A) Immunofluorescence staining of ROS in the lungs of mice after ALI treatment with different materials. (B) Immunofluorescence staining of NF-κB in the lungs of mice after ALI treatment with different materials. (C) Metabolism of PCGC in organs *in vivo* at different time.

of the lungs of the untreated LPS + PBS group mice showed obvious green fluorescence, which proved the high expression of NF-κB. After treatment, the fluorescence intensity of the other three groups decreased significantly. The PCG and curcumin groups only had weak green fluorescence, while the green fluorescence of the PCGC group almost disappeared, basically returning to the unmodeled state, which shows that PCGC can effectively reduce the protein expression of NF-κB in the lungs and basically eliminate the inflammation in the lungs, which is consistent with our previous research results. These results suggest that PCGC can be used as a nanodrug for acute inflammation *in vivo*.

3.8. *In vivo metabolism evaluation*

In order to determine the metabolism of PCGC in ALI mice, small animal fluorescence imaging system was used to evaluate the distribution of PCGC in organs (Fig. 5C). First, the fluorescent dye Cy7 was

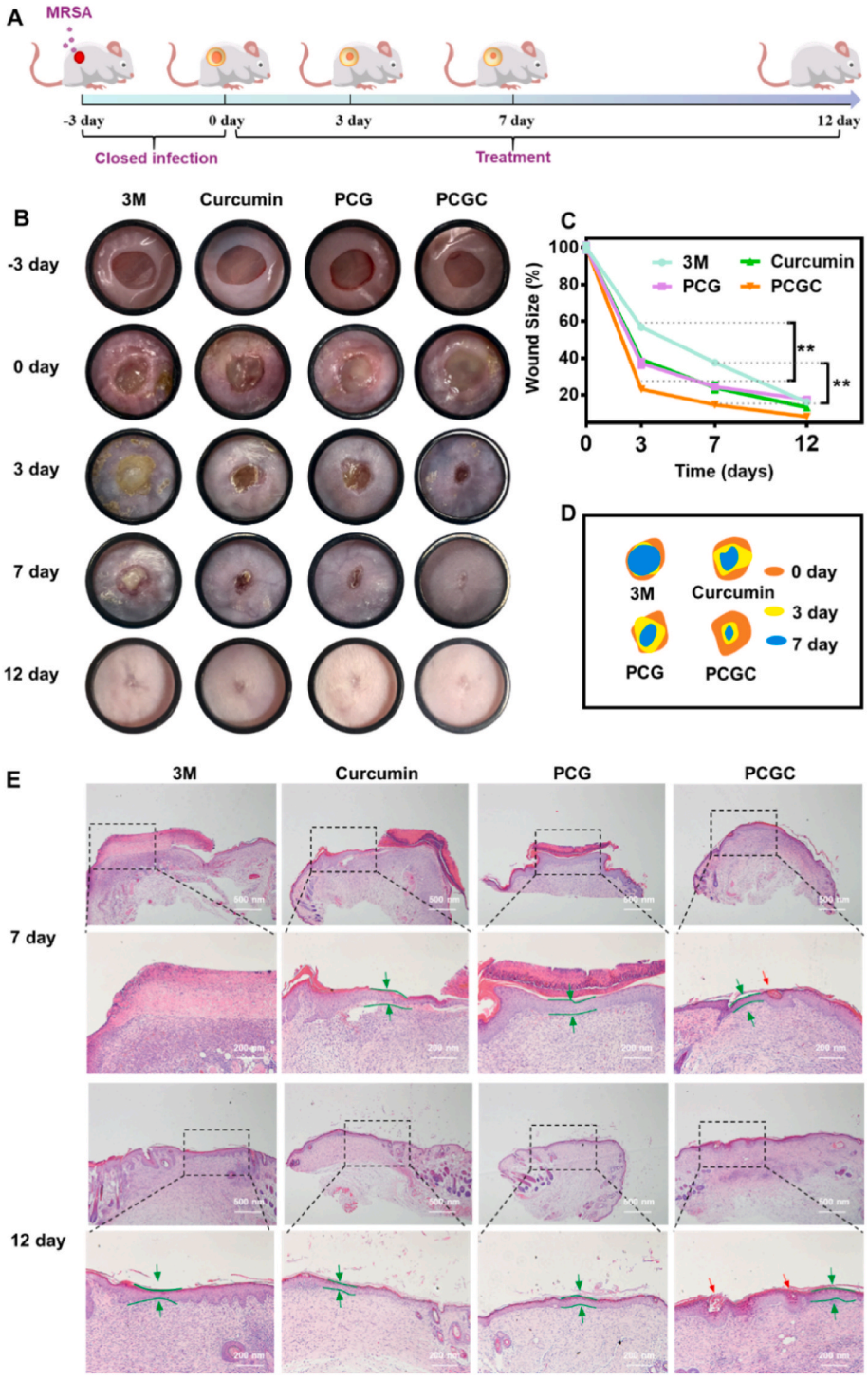

Fig. 6. Wound healing evaluation. (A) Schematic diagram of modeling mice with MRSA-infected inflammatory wound models. (B) Optical photographs of wounds on day - 3, day 0, day 3, day 7 and day 12. (C) Wound size statistics at 3, 7 and 12 days. (D) Schematic diagram of changes in wound area on day 0, 3 and 7. (E) H&E stained images of wound tissue sections at 7 days and 12 days (the first row: 4 × , the second row: 10 × , green arrows: epidermal layer, red arrows: new hair follicles).

connected to PCGC to observe the distribution of PCGC more clearly. Fig. 5C shows before the dripping of PCGC, no fluorescence was observed in each organ. After 12 h of nasal dripping of PCGC, the strongest fluorescence signal appeared in the lungs, proving that there were more PCGC distributed in the lungs at 12 h. The liver and kidneys showed weaker fluorescence. At 24 h, the fluorescence in the lungs decreased, and at 48 h, the fluorescence in the lungs weakened again. The results show that through nasal drops, PCGC can quickly reach and enrich in the lungs, and stay for more than 24 h. In addition, PCGC may be mainly metabolized through the liver and kidneys after entering the body.

3.9. MRSA-infected inflammatory wound treatment

Based on the excellent therapeutic effect of PCGC on acute inflammation in the ALI model, *Methicillin-resistant staphylococcus aureus* (MRSA)-infected inflammatory wound model was selected to further verify the anti-inflammatory therapeutic effect of PCGC (Fig. 6). The initial phase of wound healing is characterized by inflammation, and in some cases of severe infection, the inflammatory phase can be prolonged, leading to delayed healing [64]. Here, the role of PCGC in the treatment of MRSA-infected inflammatory wound was investigated (Fig. 6A). First, a circular wound with a diameter of approximately 7 mm was created on the back of the mouse (−3 day), and then MRSA was used to seal the infection for 3 days, which became an infected acute inflammatory wound (0 day). Photographs were taken at -3 -12 days to record the healing state of the wound (Fig. 6B and C). The results showed that after infection, the wound area remained unchanged, the symptoms of redness and pus appeared, and it was in the acute inflammation stage (0 day). After treating the wound for 3 days, the wound area in the 3 M group was 58.7 ± 1.9 %, and the wound was in a pus state, indicating that it was in the acute inflammation stage, and the healing speed was the slowest compared with the other groups. However, no obvious pus state was found in the CUR, PCG, and PCGC groups, and the wound area was reduced by 37.1 ± 3 %, 39.2 ± 0.8 % and 23.1 ± 0.9 %, respectively. At 3 days, the wound area of the PCGC group was the smallest, which was significantly smaller than that of the other groups, and the healing speed was the fastest. After 7 days of treatment, the wound area in the 3 M group was 37.65 ± 1.3 %, and there was still some pus. The wound area of the PCGC group was 14.65 ± 1.14 %, which was significantly smaller than that of the 3 M group, which was also because the 3 M group was still in the inflammatory phase, resulting in slow wound healing. Due to the excellent anti-inflammatory effect of PCGC, it showed an excellent effect of promoting wound healing in the early and middle stages of wound healing. On the 12th day, the wound area of the 3 M group was 16.17 ± 0.8 %. The wound surface of the 3 M group no longer presented purulent exudate at this juncture. The wound area of the curcumin, PCG, and PCGC groups was 17.58 ± 1.4 %. 13.21 ± 1.1 % and 8.17 ± 0.5 %, respectively. The 3 M group still had the largest wound area and the slowest wound healing rate, which may be due to the long period of inflammation in the early stage, which led to the prolongation of the entire healing period. The PCGC group was still the group with the smallest wound area.

Wound area is drawn and shaped at 0, 3, and 7 days to more intuitively see the changes in the wound during the healing process (Fig. 6D). According to the wound area statistics and optical state analysis, in the untreated 3 M group, prolonged inflammation resulted in continuous wound infection and pus discharge, significantly impeding wound healing speed. The PCGC treatment promoted wound healing on the 3rd, 7th, and 12th day, which shown that PCGC can greatly shorten the inflammation period through its anti-inflammatory ability and in the process of promoting wound repair.

To further explore the role of PCGC in the wound healing process, the wound tissue was collected on day 7 and 12 and judged the healing state of the wound by H&E staining (Fig. 6E). From the results of H&E staining, on the 7th day after wound infection, the 3 M group still showed an acute inflammatory state. Due to the influence of the inflammatory state, the wound in the 3 M group had not yet begun to heal, and there was no new skin or skin appendages such as hair follicles were generated, while the treated PCG, curcumin, and PCGC groups had different degrees of healing. In the process of wound healing, the epidermis undergoes a process of thickening and then thinning [65]. The inflammatory response at the wound in the PCG and curcumin groups was weakened, and the thickness of the new epidermis was thicker (green arrow), which is the state in the early stage of healing. While the inflammatory response in the PCGC group has basically disappeared, the new epidermis has begun to thin (green arrow), and hair follicles have been newly formed (red arrow). It can be considered that the PCGC group has the fastest healing rate. On the 12th day after wound infection, the wound of the 3 M group had new skin with a thicker epidermis, which was in the early stage of wound healing. Compared with that on the 7th day, the epidermis in the PCG and curcumin groups was significantly thinner, but there were no obvious new skin tissue appendages. The PCGC group had a thin epidermal layer, the fastest healing speed, multiple new hair follicles, and obvious regeneration of skin tissue attachments. Therefore, PCGC can accelerate wound healing through its anti-inflammatory effect, and at the same time, PCGC can promote tissue regeneration, which has a good effect on the entire cycle of wound healing and is promising material for promoting wound healing.

Then, immunofluorescence staining of inflammation and angiogenesis-related proteins on the collected wound tissue was performed to effect of PCGC on the wound repair (Fig. 7). The fluorescence intensity of TNF-α in 3 M group was the highest (green), indicating strong inflammation, and the fluorescence intensity of TNF-α in the other three groups was lower (Fig. 7A). Then, the fluorescence intensity was calculated. The results showed that compared with the 3 M group, the fluorescence intensity of TNF-α in the curcumin, PCG and PCGC groups was 32.1 %, 17.6 %, and 7.5 %, respectively. The expression of TNF-α in the PCGC group was the lowest, indicating that PCGC can significantly inhibited the expression of TNF-α, thus exerting a good inhibitory effect on inflammation (Fig. 7B).

VEGF is an important component of early angiogenesis in the wound healing process and the increased expression of VEGF can effectively promote wound healing [66]. VEGF immunofluorescence staining on the wound tissue collected on the 7th day was performed to judge the state of angiogenesis in each group (Fig. 6C and D). The results showed that the VEGF expression (green fluorescence) of the 3 M group was the weakest, and the fluorescence of the other groups was slightly stronger (Fig. 7C). After statistical analysis, it was found that, compared with the 3 M group, the fluorescence intensity of VEGF in the curcumin and PCG groups was 5.1 and 5.9 times that of the 3 M group, respectively, and the expression of VEGF in the PCGC group was 7.7 times that of the 3 M group (Fig. 7D). PCGC showed a strong effect of promoting the expression of VEGF, which could effectively promote wound healing through the effect of promoting angiogenesis.

The above results showed that PCGC can inhibit the expression of pro-inflammatory factor TNF-α, inhibit the infiltration of inflammatory cells, and play a role in the early stage of wound healing. On the other hand, it can promote the expression of VEGF in the middle stage of wound healing and promote angiogenesis. Finally, it can promote the regeneration of skin appendages in the middle and late stages of wound healing. Combined with anti-inflammatory, angiogenic, and pro-regenerative effects, PCGC can play a role in the entire cycle of wound healing and is an ideal wound dressing ingredient.

3.10. RNA-sequencing analysis and discussion

After confirming that PCGC has good anti-inflammatory and antioxidant effects and can play a good therapeutic role in inflammatory diseases, RAW 264.7 cells treated with PCGC were collected for transcriptome sequencing, and further explored the mechanism of PCGC in

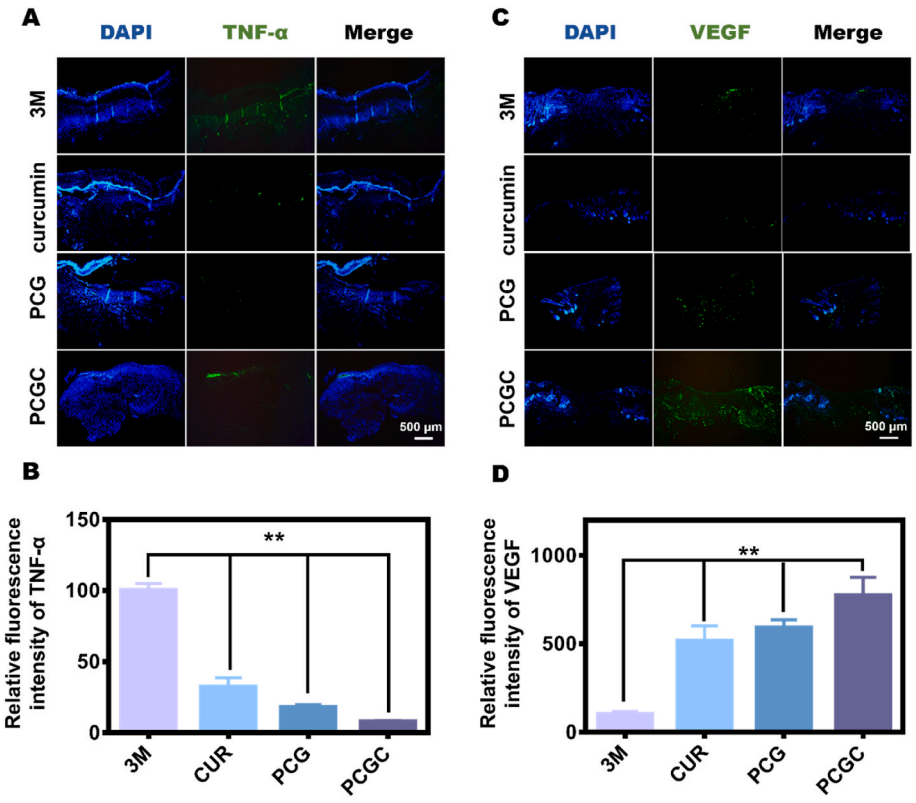

Fig. 7. Histological evaluation of the effect of 3 M, CUR, PCG and PCGC on wound healing. (A) Immunofluorescence staining of pro-inflammatory factor TNF-α in wound tissue section on the day 3, the green channel shows TNF-α expression, while the section is counterstained with DAPI. (B) The relative fluorescence intensity of TNF-α expression. (Relative to all other groups, $^{**}p < 0.01$, n = 4). (C) Immunofluorescence staining of angiogenic factor VEGF in wound tissue section on the day 7, the green channel shows VEGF expression, while the section is counterstained with DAPI. (D) The relative fluorescence intensity of VEGF expression. (Relative to all other groups, $^{**}p < 0.01$, n = 4).

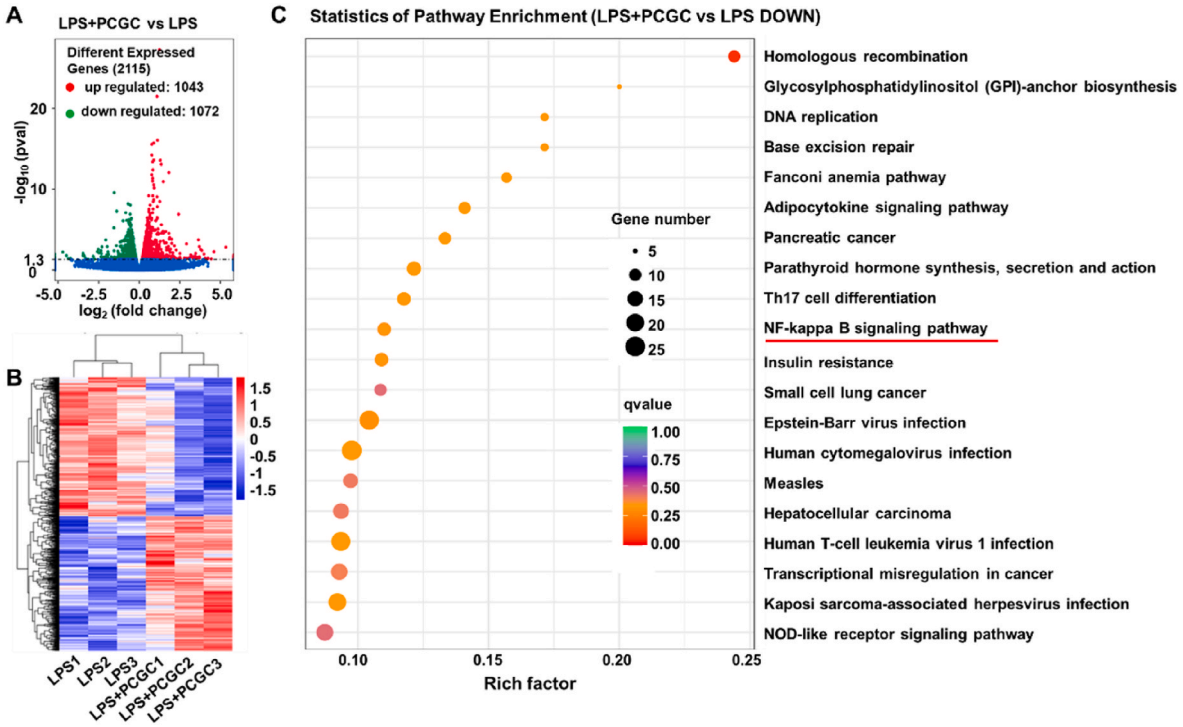

Fig. 8. Genome analysis of RAW 264.7 cells treated by PCGC. (A) Volcano plots of the total differentially expressed genes (DEGs) between LPS and LPS + PCGC groups. (B) Thermographic analysis of differentially expressed genes between LPS and LPS + PCGC groups. (C) KEGG analysis of down regulated genes.

regulating phenotypic changes in the inflammatory process. The results showed that compared with LPS group, 1043 genes were up-regulated, and 1072 genes were down-regulated in LPS + PCGC group ($p < 0.05$) (Fig. 8A). The heat map result showed the independent and average gene expression among the groups (Fig. 8B). Then the up-regulated and down-regulated genes were analyzed. Fig. 8C shows inflammation-related pathways were down-regulated after PCGC treatment. In the down-regulated pathways, some inflammation-related genes were significantly inhibited, including *TNFAIP3*, *IL*-15RA, *NF-κB*. Several genes in the *NF-κB* signal activation pathway were significantly inhibited. In conclusion, PCGC can down-regulate the inflammatory pathway, inhibit the expression of inflammatory factors, and play an excellent anti-inflammatory role.

4. Discussion

In this paper, the amphiphilic multifunctional poly (citrate-polyglycol-curcumin) (PCGC) synthesized by citrate acid (CA), 1,8-octanediol (OD), curcumin and polyethylene glycol (PEG) was reported for the first time. Compared to traditional polyester materials, PCGC has simple composition, simple synthesis procedure, low cost, and is suitable for large-scale production. The degradation products of PCGC in the body are simple, safe, and highly biologically safe. The nanoscale size of PCGC enables its uptake by macrophages and directly enter the cells for action. In addition, without adding any fluorescent dyes or quantum dots, PCGC still showed the significant photoluminescence. The fluorescence property of PCGC makes it possible to conduct real-time fluorescence imaging, locate and track the conversion process of biomaterials in inflammation treatment.

Curcumin in PCGC has very good anti-inflammatory and antioxidant effects, which has been confirmed in the current research [67,68]. However, due to its poor water solubility and high toxicity, curcumin has low bioavailability, and when applied to curcumin, it is difficult to modify it because of its high melting point [69]. In this paper, curcumin was grafted into PCGC by esterification reaction, and curcumin can be dissolved in OD during the reaction, which greatly improves the grafting rate of curcumin. Subsequently, PEG greatly improving the water solubility of PCGC. The ester bond in PCGC is hydrolyzed *in vivo*, and curcumin is released continuously and slowly, reducing the toxicity of curcumin and prolonging the action time.

CA and curcumin in PCGC have good anti-inflammatory and antioxidant effects, which enables PCGC to effectively inhibit the expression of a variety of proinflammatory factors, including *TNF-α, IL-6*, *NF-κB* and *IL-1β*, this enables PCGC to effectively inhibit the inflammatory process. In addition, PCGC can almost eliminate reactive oxygen species (ROS) in cells, which can resist oxidative damage caused by ROS and further exert anti-inflammatory effects. In acute lung injury (ALI) models, PCGC can inhibit pulmonary edema, inhibit cell infiltration in alveoli, quickly reduce lung inflammation, and have a good therapeutic effect on ALI. In *Methicillin-resistant staphylococcus aureus* (MRSA)-infected wound models, PCGC exhibits excellent healing promoting effects in the early stages, due to its anti-inflammatory and anti-oxidant effects, which inhibit the inflammatory process in the early stages of wound healing. In the middle and late stages of wound healing, PCGC promotes angiogenesis, which is because PCGC can promote the expression of vascular endothelial factor (VEGF). In previous experiments, we also found that PCGC can promote the migration of human umbilical vein endothelial cells (HUVECs), which is also crucial for angiogenesis. PCGC can also promote the growth of skin appendages, which may be attributed to curcumin can promote hair follicle growth. PCGC can promote healing and regeneration throughout the entire cycle of wound healing, making it an ideal wound dressing.

In order to study the anti-inflammatory mechanism of PCGC more clearly, LPS-treated RAW 264.7 cells treated with PCGC were collected for transcriptome sequencing, and further explored the mechanism of PCGC in regulating phenotypic changes in the inflammatory process. The results showed that PCGC up-regulated 1043 genes and down-regulated 1072 genes. Many inflammation-related pathways were down-regulated after PCGC treatment. In the down-regulated pathways, some inflammation-related genes were significantly inhibited, including *TNFAIP3, IL*-15RA, *NF-κB*. Several genes in the *NF-κB* signal activation pathway were significantly inhibited, which is basically the same as the anti-inflammatory mechanism of curcumin [70].

In summary, add active ingredients into polymers is a very effective method for preparing biomaterials. But how to add active ingredients more efficiently and maintain their biological activity is a problem that needs to be studied. The PCGC polyester platform built in this paper can be used as a new idea for the application of curcumin. In future research, we can further study whether other active ingredients can be carried for different disease treatments. In addition, the mechanism of anti-inflammatory and scavenging ROS in PCGC has not been clearly studied, and further exploration is needed in future research. There are many types of inflammatory diseases, and further exploration is needed to determine whether PCGC can still play a role in other types of inflammatory diseases.

5. Conclusion

In conclusion, we reported the amphiphilic multifunctional poly (citrate-polyglycol-curcumin) (PCGC) nanooligomers with robust inherent anti-inflammatory activity for treating acute lung injury (ALI) and *Methicillin-resistant staphylococcus aureus* (MRSA)-infected wound. PCGC could be synthesized by a facile one-pot thermal polymerization strategy and showed a typical self-assembly behavior. The presence of citrates and curcumin in the structure of PCGC enabled their robust antioxidant activity, intracellular ROS scavenging ability and antiinflammation activity. In ALI models, PCGC can effectively inhibit pulmonary edema, reduce cell infiltration in the bronchi, effectively alleviate lung inflammation, and play a rapid therapeutic role in ALI. In addition, in MRSA-infected wound, PCGC can reduce the expression of pro-inflammatory factors, promote healing in the early stage of wound healing, promote the expression of angiogenic factor VEGF to promote vascularization in the middle stage, and promote tissue regeneration and hair follicle growth in the late stage. PCGC can play a role in the entire healing process of wounds and is an ideal ingredient for wound dressings. PCGC can down-regulate multiple inflammatory pathways, especially the expression of multiple key genes in *NF-κB* pathway, which is also a specific pathway for curcumin to play an anti-inflammatory role. PCGC can also inhibit the expression of many inflammatory genes, including *TNFAIP3*, *IL*-15RA, *NF-κB*. In future work, we still need to further explore the anti-inflammatory mechanism of PCGC and explore the application of PCGC in other types of inflammation models.

Ethics approval and consent to participate

All animal experimental procedures were performed in accordance with the procedures approved by the Animal Care Committee of Xi'an Jiaotong University (2019-1167).

Declaration of interest statement

The authors declare that there is no conflict of interest for this work.

CRediT authorship contribution statement

Tongtong Leng: Writing – original draft, Methodology, Investigation, Formal analysis, Data curation. **Long Zhang:** Writing – review & editing. **Junping Ma:** Methodology, Investigation, Formal analysis. **Xiaoyan Qu:** Writing – review & editing, Supervision. **Bo Lei:** Writing – review & editing, Supervision, Funding acquisition, Conceptualization.

Acknowledgements

This work was jointly supported by the National Natural Science Foundation of China (grant No. 52172288), Young Talent Support Plan of Xi'an Jiaotong University of China (grant No. QY6J003). We thank the Instrument Analysis Center of Xi'an Jiaotong University for their assistance on characterizations.

Appendix A. Supplementary data

Supplementary data to this article can be found online at https://doi.org/10.1016/j.bioactmat.2024.07.002.

References

[1] D.D. Nguyen, J.Y. Lai, Synthesis, bioactive properties, and biomedical applications of intrinsically therapeutic nanoparticles for disease treatment, Chem. Eng. J. 435 (2022) 134970.
[2] W.D. Cruvinel, D. Mesquita, J.A.P. Araújo, T.T.T. Catelan, A.W.S. de Souza, N.P. da Silva, L.E.C. Andrade, Immune system - Part I Fundamentals of innate immunity with emphasis on molecular and cellular mechanisms of inflammatory response, Rev. Bras. Reumatol. 50 (4) (2010) 434–461.
[3] H.J. Wang, D.Z. Yang, L. Li, S.Y. Yang, G.H. Du, Y. Lu, Anti-inflammatory effects and mechanisms of rhein, an anthraquinone compound, and its applications in treating arthritis: a review, Nat. Prod. Bioprospect. 10 (6) (2020) 445–452.
[4] J.E. Woodell-May, S.D. Sommerfeld, Role of inflammation and the immune system in the progression of osteoarthritis, J. Orthop. Res. 38 (2) (2020) 253–257.
[5] P. Bortolotti, E. Faure, E. Kipnis, Inflammasomes in tissue damages and immune disorders after trauma, Front. Immunol. 9 (2018) 1900.
[6] L. Chen, H. Deng, H. Cui, J. Fang, Z. Zuo, J. Deng, Y. Li, X. Wang, L. Zhao, Inflammatory responses and inflammation-associated diseases in organs, Oncotarget 9 (6) (2018) 7204–7218.
[7] J.M. Florence, A. Krupa, L.M. Booshehri, S.A. Davis, M.A. Matthay, A. K. Kurdowska, Inhibiting Bruton's tyrosine kinase rescues mice from lethal influenza-induced acute lung injury, Am. J Physiol-Lung C 315 (1) (2018) L52–L58.
[8] D.S. James, The multisystem adverse effects of NSAID therapy, J. Am. Osteopath. Assoc. 99 (11 Suppl) (1999) S1–S7.
[9] S.M. Huang, C.S. Wu, M.H. Chiu, C.H. Wu, Y.T. Chang, G.S. Chen, C.C.E. Lan, High glucose environment induces M1 macrophage polarization that impairs keratinocyte migration via TNF-α: an important mechanism to delay the diabetic wound healing, J. Dermatol. Sci. 96 (3) (2019) 159–167.
[10] D.D. Nguyen, L.J. Luo, C.J. Yang, J.Y. Lai, Highly retina-permeating and long-acting resveratrol/metformin nanotherapeutics for enhanced treatment of macular degeneration, ACS Nano 17 (1) (2023) 168–183.
[11] C.J. Yang, D.D. Nguyen, J.Y. Lai, Poly(l-histidine)-mediated on-demand therapeutic delivery of roughened ceria nanocages for treatment of chemical eye injury, Adv. Sci. 10 (26) (2023) 2302174.
[12] C.J. Yang, A. Anand, C.C. Huang, J.Y. Lai, Unveiling the power of gabapentin-loaded nanoceria with multiple therapeutic capabilities for the treatment of dry eye disease, ACS Nano 17 (24) (2023) 25118–25135.
[13] H.J. Jian, Y.R. Chiou, A. Anand, C.F. Chen, D.H.K. Ma, J.Y. Lai, C.C. Huang, H. T. Chang, Carbon-in-carbon: hybrid carbonized nanomaterials with multifunctional activities for the treatment of endophthalmitis, Chem. Eng. J. 491 (2024) 151997.
[14] E. Burgos-Morón, Z. Abad-Jiménez, A.M. de Marañón, F. Iannantuoni, I. Escribano-López, S. López-Domènech, C. Salom, A. Jover, V. Mora, I. Roldan, E. Solá, M. Rocha, V.M. Víctor, Relationship between oxidative stress, er stress, and inflammation in type 2 diabetes: the battle continues, J. Clin. Med. 8 (9) (2019) 1385.
[15] S. Bindu, S. Mazumder, U. Bandyopadhyay, Non-steroidal anti-inflammatory drugs (NSAIDs) and organ damage: a current perspective, Biochem. Pharmacol. 180 (2020) 114147.
[16] P.A. Howard, P. Delafontaine, Nonsteroidal anti-inflammatory drugs and cardiovascular risk, J. Am. Coll. Cardiol. 43 (4) (2004) 519–525.
[17] S.F. Zhang, R. Langer, G. Traverso, Nanoparticulate drug delivery systems targeting inflammation for treatment of inflammatory bowel disease, Nano Today 16 (2017) 82–96.
[18] C.W. Li, L.L. Li, S. Chen, J.X. Zhang, W.L. Lu, Antioxidant nanotherapies for the treatment of inflammatory diseases, Front. Bioeng. Biotechnol. 8 (2020) 200.
[19] B.T. Luk, L.F. Zhang, Cell membrane-camouflaged nanoparticles for drug delivery, J. Contr. Release 220 (2015) 600–607.
[20] D.S.A. Simpson, P.L. Oliver, ROS generation in microglia: understanding oxidative stress and inflammation in neurodegenerative disease, Antioxidants-Basel 9 (8) (2020) 743.
[21] D. Yoo, C.H. Whang, J.W. Hong, D. Kim, M.C. Prayogo, Y. Son, W.S. Jung, S.J. Lee, H.S. Lee, S. Jon, Anti-inflammatory glycocalyx-mimicking nanoparticles for colitis treatment: construction and *in vivo* evaluation, Angew. Chem., Int. Ed. 62 (34) (2023) 202304815.
[22] M. Aili, K.B. Zhou, J. Zhan, H.P. Zheng, F. Luo, Anti-inflammatory role of gold nanoparticles in the prevention and treatment of Alzheime's disease, J. Mater. Chem. B 11 (36) (2023) 8605–8621.
[23] Y. Zhao, Q. Li, J.Y. Niu, E.L. Guo, C.C. Zhao, J. Zhang, X. Liu, L.H. Wang, L. Rao, X. Y. Chen, K.K. Yang, Neutrophil membrane-camouflaged polyprodrug nanomedicine for inflammation suppression in ischemic stroke therapy, Adv. Mater. (2024) 2311803.
[24] Z. Fakhari, S.N. Khorasani, F. Alihosseini, M.H.N. Esfahani, F. Karamali, S. Khalili, Core-shell nanofibers of poly (glycerol sebacate) and poly (1,8 octanediol citrate) for retinal regeneration, Polym. Bull. 79 (9) (2022) 7161–7176.
[25] J.S. Guo, X.G. Tian, D.H. Xie, K. Rahn, E. Gerhard, M.L. Kuzma, D.F. Zhou, C. Dong, X.C. Bai, Z.H. Lu, J. Yang, Citrate-based tannin-bridged bone composites for lumbar fusion, Adv. Funct. Mater. 30 (27) (2020) 2002438.
[26] Y. He, Q.Y. Li, C.Y. Ma, D.H. Xie, L.M. Li, Y.T. Zhao, D.Y. Shan, S.K. Chomos, C. Dong, J.W. Tierney, L. Sun, D. Lu, L. Gui, J. Yang, Development of osteopromotive poly (octamethylene citrate glycerophosphate) for enhanced bone regeneration, Acta Biomater. 93 (2019) 180–191.
[27] H.H. Ren, H.Y. Zhao, Y. Cui, X. Ao, A.L. Li, Z.M. Zhang, D. Qiu, Poly(1,8-octanediol citrate)/bioactive glass composite with improved mechanical performance and bioactivity for bone regeneration, Chin. Chem. Lett. 28 (11) (2017) 2116–2120.
[28] Y.W. Xi, J. Ge, Y. Guo, B. Lei, P.X. Ma, Biomimetic elastomeric polypeptide-based nanofibrous matrix for overcoming multidrug-resistant bacteria and enhancing full-thickness wound healing/skin regeneration, ACS Nano 12 (11) (2018) 10772–10784.
[29] J. Yang, A.R. Webb, G.A. Ameer, Novel citric acid-based biodegradable elastomers for tissue engineering, Adv. Mater. 16 (6) (2004) 511–516.
[30] M. Wang, P. Xu, B. Lei, Engineering multifunctional bioactive citrate-based biomaterials for tissue engineering, Bioact. Mater. 19 (2023) 511–537.
[31] Z.M. Li, G. Li, J.J. Xu, C.W. Li, S.L. Han, C.F. Zhang, P. Wu, Y.Y. Lin, C.P. Wang, J. X. Zhang, X.D. Li, Hydrogel transformed from nanoparticles for prevention of tissue injury and treatment of inflammatory diseases, Adv. Mater. 34 (16) (2022) 2109178.
[32] S.F. Zhang, J. Ermann, M.D. Succi, A. Zhou, M.J. Hamilton, B.N. Cao, J. R. Korzenik, J.N. Glickman, P.K. Vemula, L.H. Glimcher, G. Traverso, R. Langer, J. M. Karp, An inflammation-targeting hydrogel for local drug delivery in inflammatory bowel disease, Sci. Transl. Med. 7 (300) (2015) 300.
[33] Y.Z. Du, M. Yu, J. Ge, P.X. Ma, X.F. Chen, B. Lei, Development of a multifunctional platform based on strong, intrinsically photoluminescent and antimicrobial silica-poly(citrates)-based hybrid biodegradable elastomers for bone regeneration, Adv. Funct. Mater. 25 (31) (2015) 5016–5029.
[34] W.G. Liu, M. Wang, W. Cheng, W. Niu, M. Chen, M. Luo, C.X. Xie, T.T. Leng, L. Zhang, B. Lei, Bioactive antiinflammatory antibacterial hemostatic citrate-based dressing with macrophage polarization regulation for accelerating wound healing and hair follicle neogenesis, Bioact. Mater. 6 (3) (2021) 721–728.
[35] J. Su, B.H. Hu, W.L. Lowe, D.B. Kaufman, P.B. Messersmith, Anti-inflammatory peptide-functionalized hydrogels for insulin-secreting cell encapsulation, Biomaterials 31 (2) (2010) 308–314.
[36] N. Khan, H. Mukhtar, Tea polyphenols for health promotion, Life Sci. 81 (7) (2007) 519–533.
[37] D. Zhang, R. Yang, S. Wang, Z. Dong, Paclitaxel: new uses for an old drug, Drug Des. Dev. Ther. 8 (2014) 279–284.
[38] C.J. Thomas, N.J. Rahier, S.M. Hecht, Camptothecin: current perspectives, Bioorg. Med. Chem. 12 (7) (2004) 1585–1604.
[39] Y. Peng, M. Ao, B. Dong, Y. Jiang, L. Yu, Z. Chen, C. Hu, R. Xu, Anti-Inflammatory effects of curcumin in the inflammatory diseases: status, limitations and countermeasures, Drug Des. Dev. Ther. 15 (2021) 4503–4525.
[40] J.M. Zingg, S.T. Hasan, M. Meydani, Molecular mechanisms of hypolipidemic effects of curcumin, Biofactors 39 (1) (2013) 101–121.
[41] M.L. Kuo, T.S. Huang, J.K. Lin, Curcumin, an antioxidant and anti-tumor promoter, induces apoptosis in human leukemia cells, Biochim. Biophys. Acta 1317 (2) (1996) 95–100.
[42] R.K. Maheshwari, A.K. Singh, J. Gaddipati, R.C. Srimal, Multiple biological activities of curcumin: a short review, Life Sci. 78 (18) (2006) 2081–2087.
[43] P. Basnet, N. Skalko-Basnet, Curcumin: an anti-inflammatory molecule from a curry spice on the path to cancer treatment, Molecules 16 (6) (2011) 4567–4598.
[44] G.K. Jayaprakasha, L.J. Rao, K.K. Sakariah, Antioxidant activities of curcumin, demethoxycurcumin and bisdemethoxycurcumin, Food Chem. 98 (4) (2006) 720–724.
[45] M. Zhang, X.L. Zhang, T.R. Tian, Q. Zhang, Y.T. Wen, J.Y. Zhu, D.X. Xiao, W.T. Cui, Y.F. Lin, Anti-inflammatory activity of curcumin-loaded tetrahedral framework nucleic acids on acute gouty arthritis, Bioact. Mater. 8 (2022) 368–380.
[46] P. Anand, A.B. Kunnumakkara, R.A. Newman, B.B. Aggarwal, Bioavailability of curcumin: problems and promises, Mol. Pharm. 4 (6) (2007) 807–818.
[47] B.B. Aggarwal, A. Kumar, A.C. Bharti, Anticancer potential of curcumin: preclinical and clinical studies, Anticancer Res. 23 (1a) (2003) 363–398.
[48] H.J. Jian, A. Anand, J.Y. Lai, B. Unnikrishnan, H.T. Chang, S.G. Harroun, C. C. Huang, In situ hybridization of polymeric curcumin to arginine-derived carbon quantum dots for synergistic treatment of bacterial infections, ACS Appl. Mater. Interfaces 15 (22) (2023) 26457–26471.
[49] S.K. Biswas, J.B.L. De Faria, Which comes first: renal inflammation or oxidative stress in spontaneously hypertensive rats? Free Radic. Res. 41 (2) (2007) 216–224.
[50] V. Cachofeiro, M. Goicochea, S.G. de Vinuesa, P. Oubiña, V. Lahera, J. Luño, Oxidative stress and inflammation, a link between chronic kidney disease and cardiovascular disease, Kidney Int. 74 (2008) S4–S9.
[51] S.K. Biswas, Does the interdependence between oxidative stress and inflammation explain the antioxidant paradox? Oxid. Med. Cell. Longev. 2016 (2016) 5698931.
[52] J.K. Zeng, C.J. Gu, X.W. Geng, K.L. Lin, Y.Z. Xie, X.S. Chen, Combined photothermal and sonodynamic therapy using a 2D black phosphorus nanosheets

loaded coating for efficient bacterial inhibition and bone-implant integration, Biomaterials 297 (2023) 427–446.
[53] G.X. Ju, X. Liu, R.G. Li, M.T. Li, Z.Y. Qin, X.Q. Yin, Temperature-controlled release of curcumin from thermosensitive PVA/CurM nanofibrous membranes with antibacterial activity, Colloid Polym. Sci. 299 (12) (2021) 1955–1966.
[54] P. Goyal, P. Kumar, A. Gupta, Amphipathic methoxypolyethylene glycol-curcumin conjugate as effective drug delivery system useful for colonic diseases, Colloid Polym. Sci. 299 (11) (2021) 1757–1766.
[55] K.R. Ammann, K.J. DeCook, M. Li, M.J. Slepian, Migration versus proliferation as contributor to wound healing of vascular endothelial and smooth muscle cells, Exp. Cell Res. 376 (1) (2019) 58–66.
[56] W.J. Zhang, F. Yu, C.X. Yan, C.Y. Shao, P. Gu, Y. Fu, H. Sun, X.Q. Fan, PTEN inhibition accelerates corneal endothelial wound healing through increased endothelial cell division and migration, Invest. Ophthalmol. Vis. Sci. 61 (8) (2020) 19.
[57] A.M. Mahmoud, F.L. Wilkinson, M.A. Sandhu, A.P. Lightfoot, The interplay of oxidative stress and inflammation: mechanistic insights and therapeutic potential of antioxidants, Oxid. Med. Cell. Longev. 2021 (2021) 9851914.
[58] S.K. Tiwari, S. Agarwal, B. Seth, A. Yadav, S. Nair, P. Bhatnagar, M. Karmakar, M. Kumari, L.K.S. Chauhan, D.K. Patel, V. Srivastava, D. Singh, S.K. Gupta, A. Tripathi, R.K. Chaturvedi, K.C. Gupta, Curcumin-loaded nanoparticles potently induce adult neurogenesis and reverse cognitive deficits in alzheimer's disease model canonical Wnt/β-catenin pathway, ACS Nano 13 (6) (2019) 7355, 7355.
[59] A.E. Louiselle, S.M. Niemiec, C. Zgheib, K.W. Liechty, Macrophage polarization and diabetic wound healing, Transl. Res. 236 (2021) 109–116.
[60] R.Y.K. Yuan, Y.Q. Li, S. Han, X.X. Chen, J.Q. Chen, J. He, H.W. Gao, Y. Yang, S. L. Yang, Y. Yang, Fe-curcumin nanozyme-mediated reactive oxygen species scavenging and anti-inflammation for acute lung injury, ACS Cent. Sci. 8 (1) (2022) 10–21.
[61] X.M. Duan, B.W. Liu, A nanozymatic solution to acute lung injury, ACS Cent. Sci. 8 (1) (2022) 7–9.
[62] C. Liu, W.B. Fan, W.X. Cheng, Y.P. Gu, Y.M. Chen, W.H. Zhou, X.F. Yu, M.H. Chen, M.R. Zhu, K.L. Fan, Q.Y. Luo, Red emissive carbon dot superoxide dismutase nanozyme for bioimaging and ameliorating acute lung injury, Adv. Funct. Mater. 33 (19) (2023) 2213856.
[63] E.H. Lee, M.H. Shin, M. Gi, J. Park, D. Song, Y.M. Hyun, J.H. Ryu, J.K. Seong, Y. Jeon, G. Han, W. Namkung, M.S. Park, J.Y. Choi, Inhibition of Pendrin by a small molecule reduces lipopolysaccharide-induced acute lung injury, Theranostics 10 (22) (2020) 9913–9922.
[64] J. Qu, X. Zhao, Y.P. Liang, T.L. Zhang, P.X. Ma, B.L. Guo, Antibacterial adhesive injectable hydrogels with rapid self-healing, extensibility and compressibility as wound dressing for joints skin wound healing, Biomaterials 183 (2018) 185–199.
[65] W. Niu, Y. Guo, Y.M. Xue, M. Wang, M. Chen, D.D. Winston, W. Cheng, B. Lei, Biodegradable multifunctional bioactive Eu-Gd-Si-Ca glass nanoplatform for integrative imaging-targeted tumor therapy-recurrence inhibition-tissue repair, Nano Today 38 (2021) 101137.
[66] J.M. Heinzman, S.L. Brower, J.E. Bush, Comparison of angiogenesis-related factor expression in primary tumor cultures under normal and hypoxic growth conditions, Cancer Cell Int. 8 (2008) 11.
[67] J.S. Jurenka, Anti-inflammatory properties of curcumin, a major constituent of: a review of preclinical and clinical research, Alternative Med. Rev. 14 (3) (2009) 277, 277.
[68] J. Trujillo, Y.I. Chirino, E. Molina-Jijón, A.C. Andérica-Romero, E. Tapia, J. Pedraza-Chaverrí, Renoprotective effect of the antioxidant curcumin: recent findings, Redox Biol. 1 (1) (2013) 448–456.
[69] A. Jutkova, D. Chorvat, P. Miskovsky, D. Jancura, S. Datta, Encapsulation of anticancer drug curcumin and co-loading with photosensitizer hypericin into lipoproteins investigated by fluorescence resonance energy transfer, Int. J Pharm. 564 (2019) 369–378.
[70] G.W. Xu, Y.Q. Gu, N. Yan, Y.F. Li, L. Sun, B. Li, Curcumin functions as an anti-inflammatory and antioxidant agent on arsenic-induced hepatic and kidney injury by inhibiting MAPKs/NF-κB and activating Nrf2 pathways, Environ. Toxicol. 36 (11) (2021) 2161–2173.